extinguishing metaflammation: mechanisms and therapeutic opportunities for immunological control of metabolic dysfunctions

Zande, H.J.P van der

CHAPTER 7

The helminth glycoprotein omega-1 improves metabolic homeostasis in obese mice through type-2 immunity-independent inhibition of food intake

Hendrik J.P. van der Zande, Michael A. Gonzalez, Karin de Ruiter, Ruud H.P. Wilbers, Noemí García-Tardón, Mariska van Huizen, Kim van Noort, Leonard R. Pelgrom, Joost M. Lambooij, Anna Zawistowska-Deniziak, Frank Otto, Arifa Ozir-Fazalalikhan, Danny van Willigen, Mick Welling, Jordan Poles, Fijs van Leeuwen, Cornelis H. Hokke, Arjen Schots, Maria Yazdanbakhsh, P'ng Loke, Bruno Guigas

The FASEB Journal. 35:e21331. (2021)
PMID: 33476078
doi: 10.1096/fj.202001973R

Abstract

Type 2 immunity plays an essential role in the maintenance of metabolic homeostasis and its disruption during obesity promotes meta-inflammation and insulin resistance. Infection with the helminth parasite *Schistosoma mansoni* and treatment with its soluble egg antigens (SEA) induces a type 2 immune response in metabolic organs and improve insulin sensitivity and glucose tolerance in obese mice, yet a causal relationship remains unproven. Here, we investigated the effects and underlying mechanisms of the T2 ribonuclease omega-1 (ω1), one of the major *S. mansoni* immunomodulatory glycoproteins, on metabolic homeostasis. We show that treatment of obese mice with plant-produced recombinant ω1, harboring similar glycan motifs as present on the native molecule, decreased body fat mass and improved systemic insulin sensitivity and glucose tolerance in a time- and dose-dependent manner. This effect was associated with an increase in white adipose tissue (WAT) type 2 T helper cells, eosinophils and alternatively-activated macrophages, without affecting type 2 innate lymphoid cells. In contrast to SEA, the metabolic effects of ω1 were still observed in obese STAT6-deficient mice with impaired type 2 immunity, indicating that its metabolic effects are independent of the type 2 immune response. Instead, we found that ω1 inhibited food intake, without affecting locomotor activity, WAT thermogenic capacity or whole-body energy expenditure, an effect also occurring in leptin receptor-deficient obese and hyperphagic *db/db* mice. Altogether, we demonstrate that while the helminth glycoprotein ω1 can induce type 2 immunity, it improves whole-body metabolic homeostasis in obese mice by inhibiting food intake via a STAT6-independent mechanism.

Introduction

Obesity is associated with chronic low-grade inflammation in metabolic organs (1). This so-called meta-inflammation plays a prominent role in the etiology of insulin resistance and type 2 diabetes (1-3), and is associated with increased numbers of proinflammatory macrophages, notably in white adipose tissue (WAT) (4) and liver (5). In WAT, these macrophages mainly originate from newly-recruited blood monocytes that differentiate into proinflammatory macrophages upon entering the inflammatory milieu (4) and/or being activated by elevated local concentration of free fatty acids (6). These proinflammatory macrophages produce cytokines, such as tumor necrosis factor (TNF) and interleukin 1-beta (IL-1β), which directly inhibit canonical insulin signaling [as reviewed in (2)] and contribute to tissue-specific insulin resistance and whole-body metabolic dysfunctions. In the liver, activation of Kupffer cells, the tissue-resident macrophages, promote the recruitment of proinflammatory monocytes and neutrophils which trigger hepatic inflammation and insulin resistance through the production of proinflammatory cytokines and elastase, respectively (5, 7, 8). In contrast, a type 2 cytokine environment predominates in lean metabolic tissues under homeostatic conditions, notably in WAT where IL-4, IL-5 and IL-13 produced by type 2 innate lymphoid cells (ILC2s), T helper 2 (Th2) cells and/or eosinophils promote alternatively activated macrophages (AAM) (9, 10). According to the current paradigm, AAMs are the final effector cells of this type 2 immune response, contributing to the maintenance of WAT insulin sensitivity by underlying molecular mechanism(s) that are still largely unknown (2, 11).

Parasitic helminths are the strongest natural inducers of type 2 immunity (12). Interestingly, several studies have reported an association between helminth-induced type 2 immunity and improved whole-body metabolic homeostasis in both humans and rodents [(13), and as reviewed in (11)]. We also showed that chronic treatment with *S. mansoni* soluble egg antigens (SEA) promoted eosinophilia, Th2 cells, type 2 cytokines expression and AAMs in WAT, and improved both tissue-specific and systemic insulin sensitivity in obese mice (14). SEA drives dendritic cell (DC)-mediated Th2 skewing at least partly through glycosylated molecules [(15), and reviewed in (16)], particularly the T2 RNase glycoprotein omega-1 [ω1; (17, 18)]. Interestingly, acute treatment with human embryonic kidney 293 (HEK-293)-produced recombinant ω1 was recently shown to decrease body weight and improve whole-body glucose tolerance in obese mice, through ILC2-mediated type 2 immunity and induction of WAT beiging (19). In this study, the metabolic effect of ω1 was reported to be glycan-dependent, yet we have previously shown that the glycosylation pattern of HEK-293-produced ω1 differs significantly from the *S. mansoni* native molecule, which notably harbors immunogenic Lewis-X (Le^X) glycan motifs (18, 20). By exploiting the flexible N-glycosylation machinery of *Nicotiana benthamiana* plants, we successfully

produced large amounts of recombinant ω1 glycosylation variants, either carrying Le^X motifs on one of its glycan branches or not (21).

In the present study, we investigate the effects and underlying immune-dependent mechanisms of both SEA and two plant-produced ω1 glycovariants on whole-body metabolic homeostasis in obese mice. Remarkably, we demonstrate that while SEA improved metabolic homeostasis in obese mice through a STAT6-dependent type 2 immune response, recombinant pLe^X-ω1 did so independent of its type 2 immunity-inducing capacity, by reducing food intake in a leptin receptor-independent manner.

Results

S. mansoni soluble egg antigens (SEA) improve metabolic homeostasis in obese mice by a STAT6-dependent mechanism

In order to investigate the role of type 2 immunity in the beneficial metabolic effects of SEA, we used mice deficient for STAT6 (*Stat6*$^{-/-}$), a key transcription factor involved in signature type 2 cytokines interleukin (IL)-4/IL-13 signaling and maintenance of Th2 effector functions (22, 23). In line with previous studies (14, 24), we treated HFD-fed obese WT and *Stat6*$^{-/-}$ with SEA for 4 weeks (Figure 1A). We confirmed that chronic treatment with SEA increased IL-5 and IL-13-expressing Th2 cells (Figure 1B), eosinophils (Figure 1C) and $YM1^+$ AAMs (Figure 1D) in WAT from HFD-fed obese WT mice while, as expected, this type 2 immune response was abrogated in *Stat6*$^{-/-}$ mice. SEA slightly reduced body weight (Figure 1E) and similarly affected body composition (Supplementary Figure 2A) in both WT and *Stat6*$^{-/-}$ obese mice, without affecting food intake (Figure 1F). In line with our previous study, we showed that SEA reduced fasting plasma insulin levels (Supplementary Figure 2C) and HOMA-IR (Figure 1G), and improved whole-body glucose tolerance in WT obese mice (Figure 1H,J). Strikingly, this beneficial metabolic effect was completely abolished in *Stat6*$^{-/-}$ mice (Figure 1I,J), indicating that SEA improves whole-body metabolic homeostasis in obese mice through STAT6-mediated type 2 immunity.

Plant-produced recombinant ω1 glycovariants increase adipose tissue Th2 cells, eosinophils and alternatively-activated macrophages, without affecting innate lymphoid cells

One of the major type 2 immunity-inducing molecules in SEA is the T2 ribonuclease glycoprotein ω1 (18). To study the effect of ω1 on metabolic homeostasis and the role of its immunomodulatory glycans, we generated two recombinant glycosylation variants using glycol-engineered *N. benthamiana* plants: one carrying wild-type plant glycans (pWT-ω1) and one harboring terminal Le^X motifs (pLe^X-ω1;

(21)). For both ω1 glycovariants, 4 weeks treatment markedly increased WAT CD4 T cells in HFD-fed obese mice, with pWT-ω1 being slightly more potent than pLe^{X}-ω1, while total ILCs were unaffected (Figure 2A-B). Interestingly, a specific increase in WAT IL-5 and IL-13-expressing Th2 cells was seen for both ω1 glycovariants, while the other CD4 T cell subsets, *i.e.* regulatory T cells (Treg) and Th1 cells, were not affected (Figure 2C). In addition, we confirmed that HFD reduced WAT IL-5^{+}/IL-13^{+} ILC2s, as previously reported (9), an effect that was even further pronounced with ω1 glycovariants (Figure 2D). The type 2 cytokines IL-5 and IL-13 produced by either ILC2s and/or Th2 cells have been reported to maintain WAT eosinophils (9). Congruent with our data on Th2 cells, we found a potent increase in WAT eosinophils upon ω1 treatment that was of similar extent for both glycovariants (Figure 2E). Finally, both pWT-ω1 and pLe^{X}-ω1 increased WAT YM1^{+} AAMs while obesity-associated CD11c^{+} macrophages were not affected (Figure 2F-G). This ω1-induced WAT type 2 immunity was dose-dependent (Supplementary Figure 3) and already observed after one week of treatment, when ILC2s were also not affected (Supplementary Figure 4).

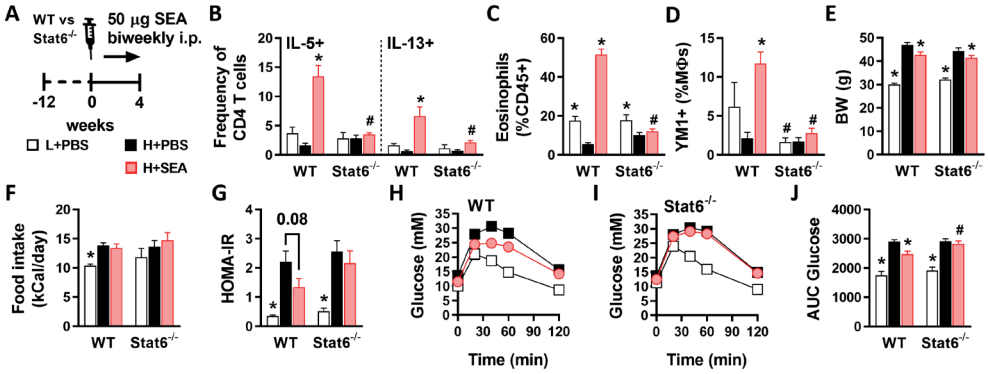

Figure 1. *S. mansoni* soluble egg antigens improve metabolic homeostasis in obese mice by a STAT6-dependent mechanism. (**A**) WT and *Stat6*$^{-/-}$ mice were fed a LFD (white bars) or a HFD for 12 weeks and next received intraperitoneal injections of PBS (black bars) or 50 µg *S. mansoni* soluble egg antigens (SEA; red bars) every 3 days for 4 weeks. At sacrifice, epididymal WAT was collected and SVF was isolated and analyzed by flow cytometry. The complete gating strategy is shown in Supplementary Figure 1. (**B**) Frequencies of IL-5 and IL-13 expressing Th2 cells in WAT were determined after PMA/ionomycin/Brefeldin A restimulation. (**C-D**) Abundances of eosinophils (*C*) and YM1^{+} macrophages (AAMs; *D*) were determined. (**E**) Body weight was measured after 4 weeks of treatment. (**F**) Food intake was monitored throughout the experimental period. (**G**) HOMA-IR was calculated using fasting blood glucose and plasma insulin levels at week 4. (**H-J**) An i.p. glucose tolerance test was performed at week 3. Blood glucose levels were measured at the indicated time points (*H-I*) and the AUC of the glucose excursion curve was calculated (*J*). Data shown are a pool of two independent experiments. Results are expressed as means ± SEM. **P*<0.05 *vs* HFD, #*P*<0.05 *vs* WT (n = 9-12 mice per group).

AAMs are considered the effector cells of WAT type 2 immunity in the maintenance of tissue insulin sensitivity (2), although the mechanisms are not fully understood. Monocyte-derived macrophages can irreversibly be labelled upon tamoxifen administration in *Cx3cr1*$^{\text{CreERT2-IRES-EYFP}}$ *Rosa26*$^{\text{LoxP-stop-LoxP-tdTomato}}$ (*Cx3cr1*$^{\text{CreER}}$ *Rosa26*$^{\text{tdTomato}}$) mice, as described elsewhere (25). In order to characterize newly recruited, ω1-induced adipose tissue macrophages (ATMs) during obesity, we performed RNA sequencing on FACS-sorted tdTomato^{+} macrophages from eWAT SVF of obese *Cx3cr1*$^{\text{CreER}}$ *Rosa26*$^{\text{tdTomato}}$ mice that were treated with PBS or pLe^{X}-ω1, the glycovariant that resembles native ω1 most (Supplementary Figure 5A). Genes associated with alternative activation, *e.g. Tmem26*, *Slc7a2, Chil3* and *Arg1*, were upregulated ($\log_2$FC > 2) in ATMs from pLe^{X}-ω1-treated mice as compared to controls, while genes associated with proinflammatory or obesity-associated macrophages, *e.g. Igfbp7, Cxcl12, Bgn, Dcn* and *Cd86*, were downregulated ($\log_2$FC < -2; Supplementary Figure 5B-C). Macrophage function is increasingly recognized to be supported by their metabolism to meet energy demands, and as such, AAMs display increased oxidative phosphorylation (26). In PD-L2^{+} WAT macrophages (Supplementary Figure 5D), pLe^{X}-ω1 indeed increased mitochondrial mass, while displaying decreased mitochondrial membrane potential and similar total reactive oxygen species production (Supplementary Figure 5E-G), a metabolic phenotype in line with alternative macrophage activation.

Similar to WAT, maintenance of insulin sensitivity in the liver is also associated with type 2 immunity (27), whereas obesity-driven activation of Kupffer cells increases the recruitment of proinflammatory monocytes and triggers hepatic insulin resistance (2, 7). In our conditions, while ω1 glycovariants increased Th2 cells in the liver, we did not find alternative activation of Kupffer cells (Supplementary Figure 6A-D). Instead, ω1 glycovariants increased the number of CD11c^{+} proinflammatory Kupffer cells (Supplementary Figure 6D), hepatic expression of proinflammatory cytokines *Ccl2, Tnf* and *Il1b* (Supplementary Figure 6E), and newly recruited monocytes (Supplementary Figure 6F), with a more potent effect in pLe^{X}-ω1-treated mice. Taken together, these data indicate that both ω1 glycovariants potently induce type 2 immunity in obese mice, triggering an alternative activation profile in WAT, but not liver macrophages.

ω1 glycovariants reduce body weight, fat mass and food intake, and improve whole-body metabolic homeostasis in obese mice

We next investigated the metabolic effects of ω1 glycovariants and showed that they both induced a rapid and gradual body weight loss in HFD-fed mice (Figure 3A-B), which was exclusively due to a decrease in fat mass (Figure 3C). The ω1 glycovariants significantly reduced visceral eWAT mass, but had no or only marginal effects on subcutaneous iWAT,

brown adipose tissue (BAT) and liver mass (Supplementary Figure 2D). This reduction in fat mass was associated with smaller adipocytes (Supplementary Figure 7A-B), reduced leptin expression (Supplementary Figure 7C-D), and opposite changes in expression of proinflammatory (decrease in *Itgax*) and alternatively-activated (increase in *Arg1*) canonical macrophage markers in both eWAT and iWAT (Supplementary Figure 7C-D). However, the lower fat mass gain was clearly not due to increased WAT beiging, as ω1 glycovariants neither increased expression of thermogenic gene markers (*Ucp1*, *Cox8b* and *Cidea*) in both eWAT and iWAT from obese mice (Supplementary Figure 7C-D), nor whole-body energy expenditure (Supplementary Figure 7E). In addition, ω1 glycovariants did not affect hepatic steatosis (Supplementary Figure 6G-I) but increased the expression of fibrotic gene markers (Supplementary Figure 8A), without detectable collagen accumulation (Supplementary Figure 8B-C). An increase in circulating alanine transaminase levels was also observed (Supplementary Figure 8D), indicating that ω1 may also have some cytotoxic effects in the liver, as previously reported (28, 29).

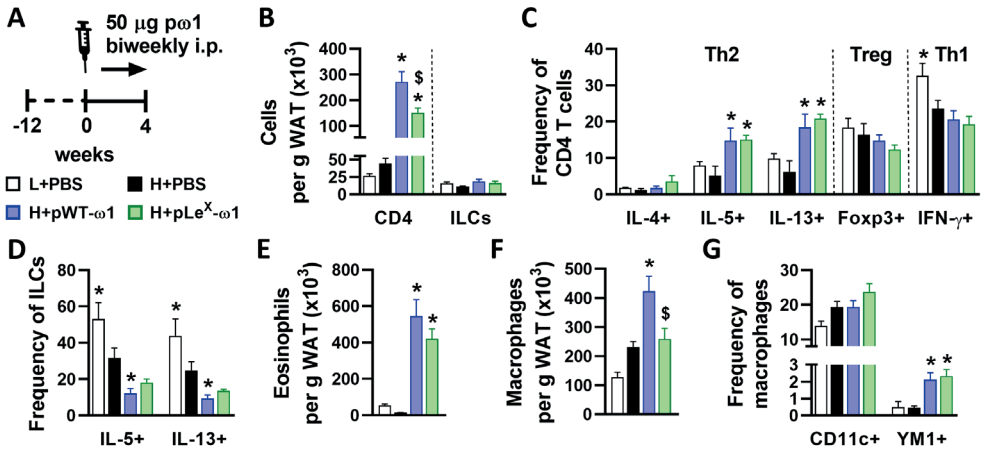

Figure 2. Plant-produced recombinant ω1 glycovariants increase adipose tissue Th2 cells, eosinophils and alternatively-activated macrophages, without affecting innate lymphoid cells. (**A**) Mice were fed a LFD (white bars) or a HFD for 12 weeks, and next received intraperitoneal injections of PBS (black bars) or either 50 µg pWT-ω1 (blue bars) or 50 µg pLe^{X}-ω1 (green bars) every 3 days for 4 weeks. At the end of the experiment, eWAT was collected, processed and analyzed as described in the legend of Figure 1. (**B-G**) Numbers of CD4 T cells, ILCs (*B*), eosinophils (*E*) and macrophages (*F*) per gram tissue were determined. Frequencies of CD4 T helper subsets (*C*) and cytokine-expressing ILCs (*D*) were determined. Percentages of CD11c^{+}YM1^{-} and CD11c^{-}YM1^{+} macrophages (*G*) were measured. Data shown are a pool of at least two independent experiments. Results are expressed as means ± SEM. **P*<0.05 *vs* HFD, $*P*<0.05 *vs* pWT-ω1 (n = 6-19 mice per group in B, E-G, and 3-9 mice per group in C and D).

Interestingly, we found that both ω1 glycovariants induced a significant decrease in food intake (Figure 3D-E), while locomotor activity was not affected (Figure 3F-G). Treatment with both ω1 glycovariants significantly reduced fasting blood glucose, plasma insulin levels (Supplementary Figure 2E-F) and HOMA-IR (Figure 3H) in obese mice, with a trend towards a stronger effect with pLe^{X}-ω1, indicating improved insulin sensitivity. Congruent with these data, we observed a significant improvement in whole-body glucose tolerance (Figure 3I-J) and insulin sensitivity (Figure 3K-L) in both pWT-ω1 and pLe^{X}-ω1-treated obese mice. Furthermore, except in eWAT, the ω1 glycovariants restored the expression the insulin receptor (IRβ) and the insulin-induced phosphorylation of PKB in the main metabolic organs, confirming enhanced insulin sensitivity (Figure 3M-P). In line with enhanced hepatic insulin sensitivity, we also found that pWT-ω1 and pLe^{X}-ω1 lowered the glucose levels during an intraperitoneal pyruvate tolerance test (Supplementary Figure 6J-K) and decreased the expression of gluconeogenic genes in the livers of obese mice (Supplementary Figure 6L), suggesting an improved insulin-induced inhibition of hepatic gluconeogenesis.

Of note, the effects of ω1 glycovariants on food intake, plasma metabolic parameters and whole-body insulin sensitivity were all dose-dependent (Supplementary Figure 3) and already observed after one week of treatment, when body weight and fat mass were only mildly affected (Supplementary Figure 4). Altogether, these data show that both recombinant ω1 glycovariants improve whole-body metabolic homeostasis in insulin-resistant obese mice.

pLe^{X}-ω1 improves metabolic homeostasis in obese mice by a STAT6-independent mechanism

We next investigated the role of type 2 immunity in the metabolic effects of ω1, using pLe^{X}-ω1 as the most potent and native-like glycovariant. As expected, while 4 weeks pLe^{X}-ω1 treatment (Figure 4A) increased WAT Th2 cells, eosinophils and YM1^{+} AAMs in obese WT mice, this type 2 immune response was abrogated in obese *Stat6*$^{-/-}$ mice (Figure 4B-D). However, treatment with pLe^{X}-ω1 still reduced body weight (Figure 4E-G) and food intake (Figure 4H), and affected body composition (Supplementary Figure 2G) in *Stat6*$^{-/-}$ obese mice to the same extent as in WT mice. In addition, both plasma insulin levels and HOMA-IR were markedly decreased in both genotypes (Supplementary Figure 2H-I and Figure 4I). The improvements in whole-body glucose tolerance (Figure 4J-L) and insulin sensitivity (Figure 4M-O) were also still observed in *Stat6*$^{-/-}$ mice, indicating that pLe^{X}-ω1's type 2 immunity-inducing capacity does not play a major role in restoration of metabolic homeostasis in obese mice. Of note, in contrast to its implication in maintenance of WAT metabolic homeostasis, IL-13 signaling has recently also been shown to play a role in the development of liver fibrosis (30, 31). Interestingly, the increase in liver IL-5^{+} and IL-13^{+}

Th2 cells in response to pLe^{X}-ω1 was also abrogated in *Stat6*$^{-/-}$ mice (Supplementary Figure 8E), and the expression of fibrotic gene markers were markedly reduced in *Stat6*$^{-/-}$ mice as compared to WT mice (Supplementary Figure 8F). Taken together, these results show that pLe^{X}-ω1 improves whole-body metabolic homeostasis independent of STAT6-mediated type 2 immunity, while promoting early markers of hepatic fibrosis at least partly through an IL-13-STAT6-mediated mechanism.

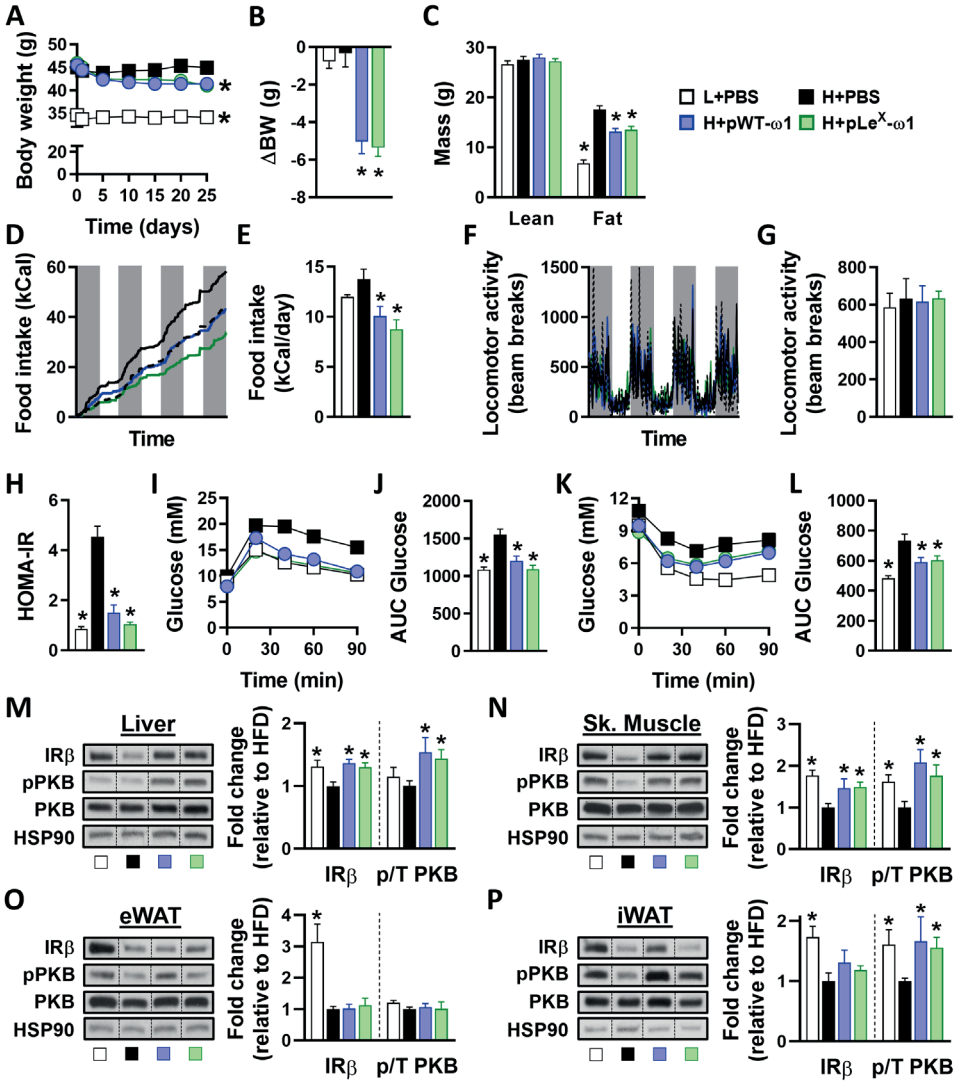

Figure 3. ω1 glycovariants reduce body weight, fat mass and food intake, and improve whole-body metabolic homeostasis in obese mice. Mice were fed a LFD (white bars) or a HFD for 12 weeks, and

▲Figure 3. Legend (Continued)

next received biweekly intraperitoneal injections of PBS (black bars) or 50 µg pWT-ω1 (blue bars) or pLe^X-ω1 (green bars) for 4 weeks. (**A-B**) Body weight was monitored throughout the experimental period. (**C**) Body composition was measured after 4 weeks of treatment. (**D-G**) Food intake (*D-E*) and locomotor activity (*F-G*) were assessed using fully automated single-housed metabolic cages during the first week of treatment. (**H**) HOMA-IR at week 4 was calculated. (**I-L**) Intraperitoneal glucose (*I-J*) and insulin (*K-L*) tolerance tests were performed during week 3. Blood glucose levels were measured at the indicated time points (*I, K*) and the AUC of the glucose excursion curve were calculated (*J, L*). (**M-P**) After 4 weeks of treatment, mice received an i.p. injection of insulin (1 U/kg lean body mass) and after 15 minutes, pieces of liver (*M*), skeletal muscle (*N*), eWAT (*O*) and iWAT (*P*) were collected and snap frozen immediately. The protein expression of IRβ and the phosphorylation state of PKB-Ser473 (pPKB) were assessed by Western blot and quantified by densitometry analysis. HSP90 expression was used as internal housekeeping protein, and phosphorylation of PKB is expressed as a ratio of phosphorylated over total PKB. Representative Western blots are shown. Data shown are a pool of at least two independent experiments. Results are expressed as means ± SEM. **P*<0.05 *vs* HFD (n = 11-20 mice per group in A-C, H-L, and 4-9 mice per group in D-G, M-P).

pLeX-ω1 improves metabolic homeostasis through leptin receptor-independent inhibition of food intake in obese mice

As ω1 significantly reduced food intake in obese mice, we next investigated its impact on feeding behavior. We found that a single intraperitoneal injection of pLe^X-ω1 in overnight fasted obese mice markedly reduced food intake during refeeding for at least 24 hours, resulting in decreased body weight gain as compared to PBS-injected mice (Figure 5A-C). To determine whether reduced food intake drives the beneficial metabolic effects of ω1, we treated HFD-fed mice with pLe^X-ω1 or PBS, and included a pair-fed group that received daily adjusted HFD meals based on the food intake of the pLe^X-ω1-treated animals (Figure 5D). While pLe^X-ω1 induced IL-13$^+$ Th2 cells, eosinophils and YM1$^+$ AAMs in WAT, reducing caloric intake in pair-fed mice did not affect WAT type 2 immunity, as expected (Figure 5E-G). Yet, food restriction in the pair-fed group decreased body weight (Figure 5H), fasting blood glucose and plasma insulin levels (Supplementary Figure 2K-L), and HOMA-IR (Figure 5I) as well as whole-body glucose tolerance to the same extent as in pLe^X-ω1-treated animals (Figure 5J-K).

The central regulation of feeding behavior and whole-body energy homeostasis involves complex neuronal networks, notably in the hypothalamus and brain stem (32, 33). To investigate whether pLe^X-ω1 accumulates in the brain to directly regulate hypothalamic neurons controlling food intake, we performed in vivo imaging experiments with pLe^X-ω1 conjugated to a hybrid tracer (^{111}In-DTPA-Cy5-pLe^X-ω1). Both Single Photo Emission Computed Tomography (SPECT) imaging and radioactivity biodistribution revealed that ^{111}In-DTPA-Cy5-pLe^X-ω1 mainly accumulated in abdominal organs, *e.g.* adipose tissues,

liver and intestines, and peritoneal draining lymph nodes, whereas no substantial amounts of radioactivity could be detected in the hypothalamus and other brain regions 24h after tracer administration (Supplementary Figure 9A-B). Of note, both glycovariants did not affect HFD-induced expression of various inflammatory genes in the whole hypothalamus (Supplementary Figure 9C), suggesting that dampening of hypothalamic inflammation is probably not involved in the anorexigenic effects of ω1. Hence, ω1 does not distribute to the brain and likely regulates food intake through peripheral effects.

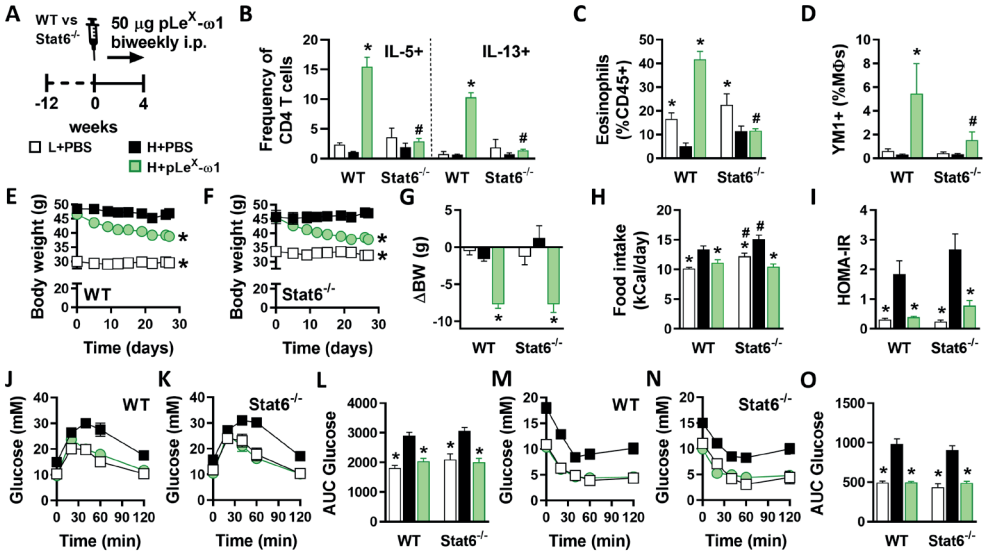

Figure 4. pLeX-ω1 improves metabolic homeostasis in obese mice by a STAT6-independent mechanism. (**A**) WT and *Stat6*$^{-/-}$ mice were fed a LFD (white bars) or a HFD for 12 weeks and next received biweekly intraperitoneal injections of PBS (black bars) or 50 µg pLe^{X}-ω1 (green bars) for 4 weeks. At the end of the experiment, eWAT was collected, processed and analyzed as described in the legend of Figure 1. (**B**) The frequencies of cytokine-expressing CD4 T cells were determined. (**C-D**) Abundances of eosinophils (*C*) and YM1^{+} macrophages (*D*) were determined. (**E-H**) Body weight (*E-G*) and food intake (*H*) were monitored throughout the experimental period. (**I**) HOMA-IR at week 4 was calculated. (**J-O**) Intraperitoneal glucose (*J-L*) and insulin (*M-O*) tolerance tests were performed as described in the legend of Figures 1 and 3. Results are expressed as means ± SEM. **P*<0.05 *vs* HFD, #*P*<0.05 *vs* WT (n = 3-5 mice per group).

The hypothalamus and brain stem also integrate signals from both the enteric nervous system and circulating hormones derived from adipose tissue and other peripheral tissues. Leptin is by far the best studied peripheral hormone that regulates food intake, increasing satiety by triggering STAT3-mediated pathways in the hypothalamic arcuate nucleus (32).

In order to study the role of leptin signaling in the metabolic effects of pLe^X-ω1, we used leptin receptor-deficient *db/db* mice that are hyperphagic and naturally develop obesity and severe metabolic dysfunctions (34). In this model, pLe^X-ω1 also increased WAT IL-13$^+$ Th2 cells, eosinophils and YM1$^+$ AAMs (Figure 6A-D). Furthermore, pLe^X-ω1 still reduced body weight (Figure 6E-F), fat mass gain (Supplementary Figure 2M-N) and food intake (Figure 6G), indicating that leptin signaling is not involved in the anorexigenic effect of ω1. Lastly, plasma insulin levels (Supplementary Figure 2P), HOMA-IR (Figure 6H) and whole-body glucose tolerance and insulin sensitivity (Figure 6I-L) were still significantly improved.

Collectively, our results show that ω1 improves whole-body metabolic homeostasis independent of its type 2 immunity-inducing capacity, but by inhibiting food intake through a leptin receptor-independent mechanism.

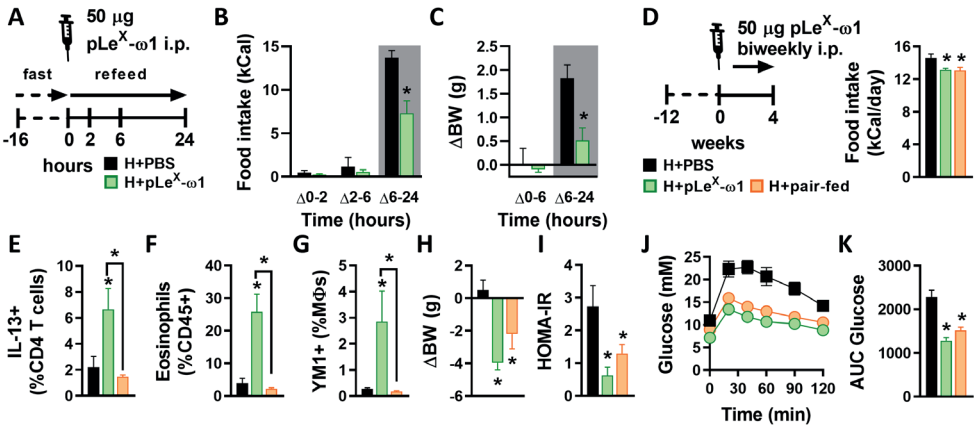

Figure 5. pLeX-ω1 inhibits fasting-induced refeeding and improves metabolic homeostasis through inhibition of food intake in obese mice. (**A**) Mice were fed a HFD for 12 weeks and fasted overnight prior to intraperitoneal injections of either PBS (black bars) or 50 µg pLe^X-ω1 (green bars). (**B-C**) Food intake (*B*) and body weight changes (*C*) were next monitored during 24 hours after refeeding. (**D**) Mice were fed a HFD for 12 weeks, single-housed, and next received biweekly intraperitoneal injections of PBS or 50 µg pLe^X-ω1 for 4 weeks. In one group (H+pair-fed; orange bars), the amount of food available for PBS-treated mice was adjusted daily in order to match the food intake of the pLe^X-ω1-treated group. At the end of the experiment, eWAT was collected, processed and analyzed as described in the legend of Figure 1. (**E-G**) The frequencies of IL-13-expressing CD4 T cells (*E*), eosinophils (*F*) and YM1$^+$ macrophages (*G*) were determined. (**H**) Body weight change was determined after 4 weeks. (**I**) HOMA-IR was calculated at week 4. (**J-K**) An i.p. glucose tolerance test was performed at week 3, as described in the legend of Figure 1. Results are expressed as means ± SEM. **P*<0.05 *vs* HFD or as indicated (n = 3-5 mice per group).

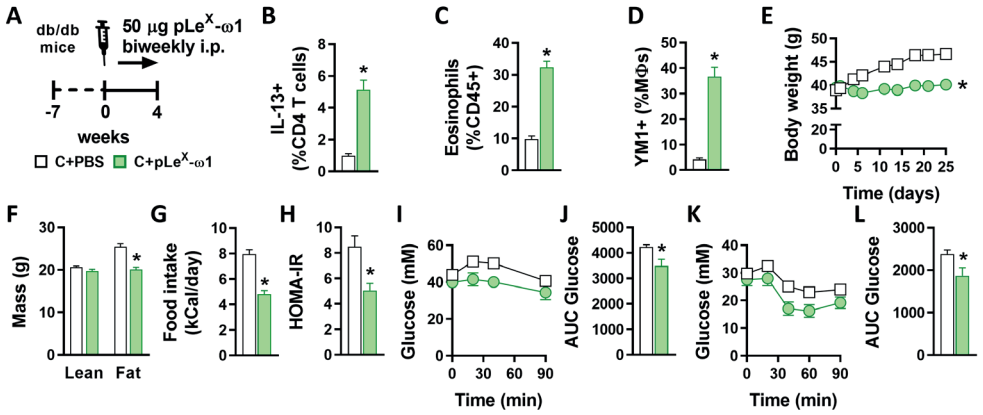

Figure 6. The metabolic effects of pLeX-ω1 are independent of leptin signaling in hyperphagic obese mice. (**A**) 7 weeks-old obese *db/db* mice received biweekly intraperitoneal injections of PBS (white bars) or 50 µg pLe^X-ω1 (green bars) for 4 weeks. At the end of the experiment, eWAT was collected, processed and analyzed as described in the legend of Figure 1. (**B-D**) The frequencies of IL-13-expressing CD4 T cells (*B*), eosinophils (*C*) and YM1$^+$ macrophages (*D*) were determined. (**E-G**) Body weight (*E*) and food intake (*G*) were monitored throughout the experimental period, and body composition (*F*) was measured after 4 weeks. (**H**) HOMA-IR was calculated at week 4. (**I-L**) Intraperitoneal glucose (*I-J*) and insulin (*K-L*) tolerance tests were performed as described in the legend of Figures 1 and 3. Results are expressed as means ± SEM. **P*<0.05 *vs* PBS (n = 5-6 mice per group).

Discussion

Obesity-associated metaflammation promotes insulin resistance, while metabolic homeostasis is maintained by type 2 immunity (1). Since helminths are well known for inducing a potent type 2 immune response, their putative beneficial effects on insulin sensitivity and glucose homeostasis, together with the identification of specific helminth-derived molecules capable of driving such type 2 immune responses, have gained increasing attention (11, 16, 35). The assumption has been that induction of type 2 immunity is the main mechanism by which helminths and helminth-derived molecules can improve metabolic homeostasis. The glycoprotein ω1, a T2 ribonuclease which is secreted from *S. mansoni* eggs, is one of the major immunomodulatory components in SEA and has previously been shown to condition DCs to prime Th2 responses, at least partly through its glycan-mediated uptake and intracellular RNase activity (17, 18). Here, we report that two plant-produced recombinant ω1 glycovariants induced a rapid and sustained reduction in body weight and improved whole-body insulin sensitivity and glucose tolerance in obese mice. This improvement was associated with a strong type 2 immune response in WAT,

characterized by a significant increase in Th2 cells, eosinophils and AAMs. Contrary to SEA, ω1 still improved metabolic homeostasis in *Stat6*-deficient obese mice, indicating that its type 2 immunity-inducing capacity does not play a major role. Indeed, we find that ω1 regulates energy consumption independent of leptin receptor signaling, which drives most of its metabolic effects. Altogether, these findings indicate that helminth-derived molecules may act through multiple distinct pathways for improving obesity-associated metabolic dysfunctions and further characterization of these molecules may lead to new therapeutic strategies for combating obesity.

A recent study from Hams et al. also reported that acute treatment of HFD-fed obese mice with HEK-293-produced recombinant ω1 induced long-lasting weight loss, and improved glucose tolerance by a mechanism involving IL-33 and ILC2-mediated WAT type 2 immunity and adipose tissue beiging (19). In contrast to this report, while we also observed increased IL-33 mRNA expression in eWAT using the same ω1 concentrations (*data not shown*), we found no increase in WAT ILC2s after either one, or four weeks of treatment with both plant-produced ω1 glycovariants. Moreover, we did not find evidence of WAT beiging in both eWAT and iWAT from obese mice. Lastly, we also found that STAT6-mediated type 2 immunity was dispensable for the metabolic effects of ω1. It should be noted that despite similar RNase activity when compared to native ω1 (21), the recombinant ω1 produced by HEK-293 cells and the glyco-engineered molecules from *N. benthamiana* plants harbor significantly different N-glycosylation patterns (18), which may partly explain the different outcomes between studies. Interestingly, as compared to pWT-ω1, we observed a trend for a stronger effect on insulin sensitivity and food intake with pLe^X-ω1, of which the glycans resemble the ones of native helminth ω1 the most.

In our study, both ω1 glycovariants were found to induce a type 2 immune response in WAT, characterized by a significant increase in Th2 cells, eosinophils and AAMs. WAT eosinophilia is dependent on IL-5 and IL-13, which are predominantly expressed by ILC2s, and, to a lower extent, by Th2 cells in lean mice (9). As previously described for SEA (14), we showed that the ω1-induced increase in type 2 cytokines is clearly derived from CD4$^+$ T cells, suggesting that DC-mediated Th2 skewing is required, rather than ILC2 activation, to induce WAT eosinophilia and AAM polarization. Of note, it was previously shown that pLe^X-ω1, compared to pWT-ω1, induced a stronger Th2 polarization *in vivo* using a footpad immunization model in mice (21). In our conditions, both glycovariants induced a similar increase in the percentage of Th2 cells in metabolic tissues from obese mice, whereas pLe^X–ω1 increased total CD4$^+$ T cells to a greater extent in the liver and to a lesser extent in WAT when compared to pWT-ω1. Altogether, this suggests that the different glycans on ω1 glycovariants might lead to tissue-specific targeting of ω1 and resulting differences in total Th2 cells.

While the type 2 immune response seems not to be significantly involved in the beneficial metabolic effects of ω1, we found that treatment with both ω1 glycovariants reduced food intake, with a trend for pLe^X-ω1 being more potent than pWT-ω1. This anorexigenic effect, which was not observed previously when mice were chronically infected with *S. mansoni* or treated with SEA [Figure 1F and (14)], was dose-dependent and also observed in *Stat6*-deficient mice. Importantly, since both locomotor activity and lean body mass were not affected by ω1, this inhibition of food intake is unlikely to be caused by illnesses associated with catatonia. Using fast-refeeding and paired feeding experiments, we clearly showed that ω1 rapidly inhibited food intake, an effect that mainly contributed to the improvements in metabolic homeostasis. This inhibition of food intake persisted throughout the four weeks of treatment, indicating a long-lasting effect, and was already achieved by injecting 10 µg pLe^X-ω1 (*data not shown*). Of note, in the study from Hams *et al.* using HEK-produced recombinant ω1 in the same concentration range as us, the effect of ω1 on feeding behavior and its putative contribution to the observed decrease in body weight and improvement of glucose tolerance in obese mice have not been specifically investigated (19).

Anorexia is one of the clinical manifestations of infection with different helminth species in both animals and humans. As such, deworming children infected with the hookworms *Ascaris lumbricoides* and/or *Trichuris trichuria* has been reported to increase appetite (36), suggesting a relationship between helminth infection and food intake. In rodents, infection with *Taenia taeniaformis* and *N. brasiliensis* both induced anorexia by modulating neuropeptide expression in the hypothalamus (37, 38), indicating that helminths and/or helminth products may regulate feeding behavior. The mechanism by which ω1 inhibits food intake is however still unknown and will require further neuroscience-driven approaches to be elucidated. Regulation of food intake by the central nervous system is a complex process involving both local and peripheral neuro-immuno-endocrine inputs that are mainly integrated in the hypothalamic arcuate nucleus and the brain stem *nucleus tractus solitarius* (32, 33). In our study, we did not detect accumulation of radioactively-labelled ω1 in the brain 24 hours after intraperitoneal injection, suggesting that the glycoprotein may exerts its anorexigenic effects via peripheral rather than central action(s). Upon meal ingestion, several anorexigenic peptides and hormones are produced by metabolic organs, including adipose tissues and the intestine, and can either directly act on specific neurons after crossing the blood-brain barrier or signal from the periphery via vagal nerve-mediated pathways that contribute to satiety regulation (39, 40). Leptin is a key adipose tissue-derived anorexigenic hormone which signals through the leptin receptor expressed in specific neurons located in the arcuate nucleus of the hypothalamus to reduce food intake (32). During obesity,

hypothalamic inflammation has been reported to impair whole-body energy homeostasis, at least partly by inducing central leptin resistance and subsequent increased food intake (41-43). However, despite some evidence of improved systemic leptin sensitivity by ω1 (data not shown), we showed that the hypothalamic expression of key inflammatory genes was not affected by ω1 in obese mice, suggesting that modulation of hypothalamic inflammation is likely not involved in its anorexigenic effect. Furthermore, we found that its anorexigenic and metabolic effects were still present in leptin receptor-deficient mice, allowing us to exclude a significant contribution of peripheral/central leptin signaling. Among the peripheral signals that regulate feeding behavior, it would be interesting to explore the involvement of a gut-brain axis, potentially secondary to changes in gut microbiota, through vagal nerve ablation (40). Recently, *N. brasiliensis* infection and its products were also shown to increase production of the neuropeptide Neuromedin U by mucosal neurons, allowing the host to mount an effective type 2 immune response (44-46). Neuromedin U also has anorexigenic effects (47), thus it is tempting to speculate that some helminth molecules may indirectly trigger anorexia through neuro-immune interactions in the gut.

It is worth mentioning that ω1 also increased IL-13 producing Th2 cells in the liver, but, unlike SEA (14), promoted CD11c expression in Kupffer cells while not affecting the expression of YM1, suggesting that macrophages are rather polarized towards a proinflammatory state in this tissue. An increase in hepatic expression of fibrotic gene markers and circulating ALAT levels was also observed, both indicating increased liver damage induced by ω1. Interestingly, the ω1-induced increase in IL-13$^+$ Th2 cells and IL-13 gene expression in the liver were markedly reduced in *Stat6*-deficient mice, which was accompanied by a decreased expression of fibrotic gene markers. Collectively, these findings confirmed previous studies describing that IL-13 plays a role in the development of liver fibrosis (30, 31), and that ω1 has cytotoxic effects in the liver (28, 29).

In conclusion, we report here that the helminth glycoprotein ω1 improved metabolic homeostasis in insulin-resistant obese mice independent of its type 2 immunity-inducing capacity. Rather, the ω1-induced metabolic improvements in obese mice were mostly attributable to leptin receptor-independent inhibition of food intake. Further studies are required to unravel such underlying mechanisms, notably exploring the role of gut hormones on peripheral and/or central regulation of feeding behavior. Of note, with regards to its putative therapeutic potential for metabolic disorders, it is important to underline that despite beneficial effects on whole-body metabolic homeostasis, ω1 also induced early markers of mild hepatic fibrosis, partly through a type 2 immunity-mediated mechanism. Finally, by contrast to ω1, the complex mixture of SEA does not have detrimental effects on the liver and improves metabolic homeostasis through a STAT6-mediated type 2 immune

response, suggesting that it may contain some other unidentified molecules, such as Dectin 2 ligands (48), with potentially beneficial immunometabolic properties.

Methods

Animals, diet and treatment

All mouse experiments were performed in accordance with the Guide for the Care and Use of Laboratory Animals of the Institute for Laboratory Animal Research and have received approval from the university Ethical Review Board (Leiden University Medical Center, Leiden, The Netherlands; DEC12199) or the Institutional Animal Care and Use Committee (IACUC, New York University School of Medicine, New York, USA; protocol ID IA16-00864). All mice were housed in a temperature-controlled room with a 12-hour light-dark cycle with *ad libitum* access to food and tap water. Group randomization was systematically performed before the start of each experiment, based on body weight, fat mass, and fasting plasma glucose levels. At the end of the experiment, mice were sacrificed through an overdose of ketamine/xylazine.

8-10 weeks old male wild-type (WT) and 7 weeks old male *db/db* mice, both on C57BL6/J background, were purchased from Envigo (Horst, The Netherlands) and housed at Leiden University Medical Center. WT mice were fed a low-fat diet (LFD, 10% energy derived from fat, D12450B, Research Diets, Wijk bij Duurstede, The Netherlands) or a high-fat diet (HFD, 45% energy derived from fat, D12451) for 12 weeks, and *db/db* mice were fed a chow diet (RM3 (P), Special Diet Services, Witham, UK) throughout the experimental period.

8-10 weeks-old male wild-type (WT), *Stat6*$^{-/-}$ mice and *Rosa26*$^{\text{LoxP-STOP-LoxP-tdTomato/+}}$ (*Rosa26*$^{\text{tdTomato}}$), were purchased from The Jackson Laboratory (Bar Harbor, ME, USA), and *Cx3cr1*$^{\text{CreERT2-IRES-YFP/+}}$ (*Cx3cr1*$^{\text{CreER}}$) mice, all on C57BL/6J background, were generously provided by Dr. Dan Littman (Skirball Institute, New York University Medical Center). Mice were housed at New York University School of Medicine, and either put on a HFD (60% energy derived from fat; D12492; Research Diets, New Brunswick, NJ, USA) or LFD (10% energy derived from fat; D12450J; Research Diets) for 10 weeks. To exclude effects of genotype-dependent microbiota differences on metabolic and immunological outcomes, the beddings of WT and *Stat6*$^{-/-}$ mice were frequently mixed within similar diet groups throughout the run-in period. At 14 days and 7 days before sacrifice, *Cx3cr1*$^{\text{CreER}}$ *Rosa26*$^{\text{tdTomato}}$ reporter mice received an oral gavage with tamoxifen to label monocytes.

SEA was prepared as described previously (49). Recombinant ω1 was produced in *N. benthamiana* plants through transient expression of ω1 alone (pWT-ω1) or ω1 in combination with exogenous glycosyltransferases to yield Le^X glycan motifs (pLe^X-ω1), as

described previously (21). SEA, pWT/pLe^X-ω1 (10-50 μg) or vehicle control (sterile-filtered PBS) were injected i.p. every 3 days for 1 or 4 weeks, as indicated in the legends of the figures. For fast-refeeding experiments, WT HFD-fed mice received an i.p. injection of 50 μg pLe^X-ω1 or vehicle control after an overnight fast (5pm-9am), followed by refeeding and frequent measurements of food intake and body weight for 24 hours. For assessing the contribution of reduced food intake on the immunometabolic effects of pLe^X-ω1, WT HFD-fed mice were single-housed and, in a pair-fed group of PBS-injected mice, daily food availability was adjusted to the calorie intake of the pLe^X-ω1-treated group.

Body composition and indirect calorimetry

Body composition was measured by MRI using an EchoMRI (Echo Medical Systems, Houston, TX, USA). Groups of 4-8 mice with free access to food and water were subjected to individual indirect calorimetric measurements during the initiation of the treatment with recombinant ω1 for a period of 7 consecutive days using a Comprehensive Laboratory Animal Monitoring System (Columbus Instruments, Columbus, OH, USA). Before the start of the measurements, single-housed animals were acclimated to the cages for a period of 48 hours. Feeding behavior was assessed by real-time food intake. Oxygen consumption and carbon dioxide production were measured at 15-minute intervals. Energy expenditure (EE) was calculated and normalized for lean body mass (LBM), as previously described (14). Spontaneous locomotor activity was determined by the measurement of beam breaks.

At sacrifice, visceral white adipose tissue (epididymal; eWAT), subcutaneous white adipose tissue (inguinal; iWAT), supraclavicular brown adipose tissue (BAT) and liver were weighed and collected for further processing and analyses.

Isolation of stromal vascular fraction from adipose tissue

eWAT was collected at sacrifice after a 1-minute perfusion with PBS through the heart left ventricle and digested as described previously (14). In short, collected tissues were minced and incubated for 1 hour at 37°C in an agitated incubator (60 rpm) in HEPES buffer (pH 7.4) containing 0.5 g/L collagenase type I from *Clostridium histolyticum* (Sigma-Aldrich, Zwijndrecht, The Netherlands) and 2% (w/v) dialyzed bovine serum albumin (BSA, fraction V; Sigma-Aldrich). The disaggregated adipose tissue was passed through a 100 μm cell strainer that was washed with PBS supplemented with 2.5 mM EDTA and 5% FCS. After centrifugation (350 x g, 10 minutes at room temperature), the supernatant was discarded and the pellet was treated with erythrocyte lysis buffer (0.15 M NH_4Cl; 1 mM $KHCO_3$; 0.1 mM Na_2EDTA). Cells were next washed with PBS/EDTA/FCS, and counted manually.

Isolation of leukocytes from liver tissue

Livers were collected and digested as described previously (14). In short, livers were minced and incubated for 45 minutes at 37°C in RPMI 1640 + Glutamax (Life Technologies, Bleiswijk, The Netherlands) containing 1 mg/mL collagenase type IV from *C. histolyticum*, 2000 U/mL DNase (both Sigma-Aldrich) and 1 mM $CaCl_2$. The digested liver tissues were passed through a 100 µm cell strainer that was washed with PBS/EDTA/FCS. Following centrifugation (530 x g, 10 minutes at 4°C), the supernatant was discarded, after which the pellet was resuspended in PBS/EDTA/FCS and centrifuged at 50 x g to pellet hepatocytes (3 minutes at 4°C). Next, supernatants were collected and pelleted (530 x g, 10 minutes at 4°C). The cell pellet was first treated with erythrocyte lysis buffer and next washed with PBS/EDTA/FCS. $CD45^+$ leukocytes were isolated using LS columns and CD45 MicroBeads (35 µL beads per liver, Miltenyi Biotec) according to manufacturer's protocol and counted manually.

Processing of isolated immune cells for flow cytometry

For analysis of macrophage and lymphocyte subsets, both WAT stromal vascular cells and liver leukocytes were stained with the live/dead marker Aqua (Invitrogen, Bleiswijk, The Netherlands) or Zombie-UV (Biolegend, San Diego, CA, USA), fixed with either 1.9% formaldehyde (Sigma-Aldrich) or the eBioscience™ FOXP3/Transcription Factor Staining Buffer Set (Invitrogen), and stored in FACS buffer (PBS, 0.02% sodium azide, 0.5% FCS) at 4°C in the dark until subsequent analysis. For analysis of cytokine production, isolated cells were cultured for 4 hours in culture medium in the presence of 100 ng/mL phorbol myristate acetate (PMA), 1 µg/mL ionomycin and 10 µg/mL Brefeldin A (all from Sigma-Aldrich). After 4 hours, cells were washed with PBS, stained with Aqua, and fixed as described above.

Flow cytometry

For analysis of CD4 T cells and innate lymphoid cell (ILC) subsets, SVF cells were stained with antibodies against B220 (RA3-6B2), CD11b (M1/70), CD3 (17A2), CD4 (GK1.5), NK1.1 (PK136) and Thy1.2 (53-2.1; eBioscience), CD11c (HL3) and GR-1 (RB6-8C5; both BD Biosciences, San Jose, CA, USA), and CD45.2 (104; eBioscience, Biolegend or Tonbo Biosciences, San Diego, CA, USA). CD4 T cells were identified as $CD45^+$ $Thy1.2^+$ $Lineage^+$ $CD4^+$, and ILCs as $CD45^+$ $Thy1.2^+$ $Lineage^-$ $CD4^-$ cells, in which the lineage cocktail included antibodies against CD11b, CD11c, B220, GR-1, NK1.1 and CD3.

CD4 T cell subsets and cytokine production by ILCs were analyzed following permeabilization with either 0.5% saponin (Sigma-Aldrich) or eBioscience™ FOXP3/ Transcription Factor Staining Buffer Set. Subsets were identified using antibodies against CD11b, CD11c, GR-1, B220, NK1.1, CD3, CD45.2, CD4, Thy1.2, IL-4 (11B11), IL-13 (eBio13A), Foxp3 (FJK-16s; all eBioscience), IL-5 (TRFK5) and IFN-γ (XMG1.2; both Biolegend).

For analysis of macrophages, eosinophils, monocytes and neutrophils, cells were permeabilized as described above. Cells were then incubated with an antibody against YM1 conjugated to biotin (polyclonal; R&D Systems, Minneapolis, MN, USA), washed, and stained with streptavidin-PerCP (BD Biosciences) or streptavidin-PerCP-Cy5.5 (Biolegend), and antibodies directed against CD45 (30-F11, Biolegend), CD45.2, CD11b, CD11c [HL3 (BD Biosciences) or N418 (Biolegend)], F4/80 (BM8; Invitrogen or Biolegend), Siglec-F (E50-2440; BD Biosciences), and Ly6C (HK1.4; Biolegend).

Mitochondrial mass, membrane potential and total ROS were quantified by staining with MitoTracker Green (20 nM), Tetramethylrhodamine, Methyl Ester, Perchlorate (TMRM; 20 nM) and CM-H2DCFDA (5 μM; all Invitrogen), respectively, for 30 minutes at 37°C before staining with other antibodies. For sorting adipose tissue macrophages, cells were stained with the live/dead marker Blue, followed by staining for surface markers. Macrophages were fluorescence-assisted cell sorted from adipose tissue on an Aria II cell sorter (BD Biosciences), by gating on singlet, live, $CD45.2^+$ $Ly6C^-$ $CD3^-$ $CD19^-$ $NK1.1^-$ $Siglec\text{-}F^-$ $CD11b^+$ $F4/80^+$ $tdTomato^+$.

All cells were stained and measured within 4 days post fixation. Flow cytometry was performed using a FACSCanto or LSR-II (both BD Biosciences), and gates were set according to Fluorescence Minus One (FMO) controls. Representative gating schemes are shown in Supplementary Figure 1 and all antibodies used are listed in Supplementary Table 1.

Plasma analysis

Blood samples were collected from the tail tip of 4h-fasted mice (food removed at 9 am) using chilled paraoxon-coated capillaries. Fasting blood glucose level was determined using a Glucometer (Accu-Check; Roche Diagnostics, Almere, The Netherlands) and plasma insulin level was measured using a commercial kit according to the instructions of the manufacturer (Chrystal Chem, Zaandam, The Netherlands). The homeostatic model assessment of insulin resistance (HOMA-IR) adapted to mice (50) was calculated as ([glucose (mg/dl)*0.055] × [insulin (ng/ml) × 172.1])/3857, and used as a surrogate measure of whole-body insulin resistance. Plasma concentrations of alanine aminotransferase (ALAT) were measured using

a Reflotron® kit (Roche diagnostics) using a pool of plasma samples from each group (n = 4-6 mice per group) in 2 separate experiments.

Glucose, insulin and pyruvate tolerance tests

Whole-body glucose tolerance test (ipGTT) was performed at week 3 of treatment in 6h-fasted mice, as previously reported (14). In short, after an initial blood collection by tail bleeding (t = 0), a glucose load (2 g/kg total body weight of D-Glucose [Sigma-Aldrich]) was administered i.p., and blood glucose was measured at 20, 40, 60, and 90 min after glucose administration using a Glucometer. For *db/db* mice, blood samples were collected at 0, 20, 40 and 90 min after glucose administration, and plasma glucose levels were measured using the hexokinase method (HUMAN, Wiesbaden, Germany).

Whole-body insulin tolerance test (ipITT) was performed at week 1 or week 3 of treatment in 4h-fasted mice, as described previously (14). In short, after an initial blood collection by tail bleeding (t = 0), a bolus of insulin (1 U/kg (lean) body mass [NOVORAPID, Novo Nordisk, Alphen aan den Rijn, Netherlands]) was administered i.p., and blood glucose was measured at 20, 40, 60, and 90 min after insulin administration using a Glucometer.

Whole-body pyruvate tolerance test (ipPTT) was performed at week 4 of treatment in overnight-fasted mice. In short, after an initial blood collection by tail bleeding (t = 0), a pyruvate load (2 g/kg total body weight of sodium pyruvate [Sigma-Aldrich]) was administered i.p. Blood glucose was measured at 20, 60, 90 and 120 min after pyruvate administration using a Glucometer.

Western blot analysis

A piece of liver, skeletal muscle, eWAT and iWAT from mice that were sacrificed 15 min after an acute i.p. injection of insulin (1 U/kg lean body mass, NOVORAPID, Novo Nordisk, Alphen aan den Rijn, Netherlands) was collected and immediately freeze-clamped. Snap-frozen samples (~50 mg) were lysed in ice-cold buffer containing: 50 mM HEPES (pH 7.6), 50 mM NaF, 50 mM KCl, 5 mM NaPPi, 1 mM EDTA, 1 mM EGTA, 1 mM DTT, 5 mM β-glycerophosphate, 1 mM sodium vanadate, 1% NP40 and protease inhibitors cocktail (Complete, Roche, Mijdrecht, The Netherlands). Western blots were performed as previously described (51). The primary antibodies used were pSer473-PKB (#9271, Cell Signaling Technology), PKB (#4691, Cell Signaling Technology), IRb (sc-711, Santa Cruz Biotechnology) and HSP90 (sc-7947, Santa Cruz Biotechnology). Bands were visualized by enhanced chemiluminescence and quantified using Image J (NIH, US).

RNA isolation and qRT-PCR

RNA was extracted from snap-frozen adipose tissue and liver samples using Tripure RNA Isolation reagent (Roche Diagnostics). Total RNA (1 μg) was reverse transcribed and quantitative real-time PCR was performed with SYBR Green Core Kit on a MyIQ thermal cycler (Bio-Rad) using specific primers sets (available on request). mRNA expression was normalized to ribosomal protein, large, P0 (*RplP0*) mRNA content and expressed as fold change compared to LFD-fed or HFD-fed mice as indicated, using the ΔΔCT method.

Transcriptomic analysis by RNA-sequencing

RNA isolation from FACS-purified adipose tissue macrophages was done as described previously with the QIAGEN RNeasy micro kit (QIAGEN, Venlo, the Netherlands) (25). Libraries were generated for each sample using the CelSeq2 protocol (52) and were sequenced on Illumina HiSeq. Reads were mapped by Bowtie2.3.1 (53) to the *mus musculus* reference genome, and uniquely mapped indices were determined by HTSeq-counts (54). Gene read counts were normalized to *B2m* and *Rplp0*. Transcriptome data was visualized with an MA-plot. Upregulated (log_2 fold change > 2 *vs* HFD) and downregulated (log_2 fold change < -2 *vs* HFD) genes were visualized in a heat map using the online software tool Morpheus (https://software.broadinstitute.org/morpheus).

Hepatic triglyceride content

Liver lipids were extracted as previously described (55). Briefly, ~50 mg liver samples were homogenized in 10:1 (vol/wt) ice-cold methanol using a FastPrep-24 5GTM High Speed Homogenizer (MP Biomedicals, Santa Ana, CA, USA). Subsequently, lipids were extracted from the homogenate using methanol-chloroform (1:3 v/v) extraction. Protein concentration of the homogenate was determined by Pierce™ BCA protein assay (Thermo Fisher Scientific). Triglyceride (TG) of the lipid extract were determined using a commercially available kit (Roche Diagnostics).

Histological analysis

A piece of liver was fixed in 4% formaldehyde (Sigma-Aldrich), paraffin-embedded, sectioned at 4 μm and stained with Hematoxylin and Eosin (H&E), or Sirius Red to visualize collagen. Six fields at 20x magnification (total area 1.68 mm^2) were used for the analysis of hepatic steatosis in H&E-stained sections. On Sirius Red-stained sections, fibrosis was scored on 10 fields at 40x magnification (total area 1.23 mm^2) as absent (score 0), present in the

perisinusoidal or periportal area (score 1), present in the perisinusoidal and periportal (score 2), bridging fibrosis (score 3) or cirrhosis (score 4) as described elsewhere (56).

Biodistribution of pLe^X-ω1

Synthesis of N3-Cy5-pLeX-ω1

DTPA-DBCO click chelate and Cy5-N_3 dye were synthesized as described previously (57), with one deviation for Cy5-N_3 synthesis being the use of 1-(5-carboxypentyl)-2,3,3-trimethyl-3H-indol-1-ium-5-sulfonate instead of 1-(5-carboxypentyl)-2,3,3-trimethyl-3H-indol-1-ium. Cy5-N_3 molecular mass was calculated to be 823.8 and found to be 824.0 using MALDI-TOF (Bruker, Leiderdorp, Netherlands). To allow for N_3-Cy5-pLe^X-ω1 formation, 200 µL of phosphate buffer (100 mM, pH 8.5) was added to 200 µg (6.5 nmol) pLe^X-ω1 (1.9 mg/mL in PBS), followed by 9.5 µL (58.1 nmol) of Cy5-N_3 (5 mg/mL stock solution in DMSO). After mixing for 60 minutes at room temperature, 90 µL of PBS was added and the unreacted Cy5 was removed using a PD MiniTrap G-25 column (Merck KGaA, Darmstadt, Germany). The labelling ratio was estimated to be 0.9 dye/protein using UV/Vis spectroscopy (Nanodrop) and the eluate (1 mL) was stored at 7°C prior to use.

Radiolabeling of pLeX-ω1

DTPA-DBCO (2.6 nmol) was dissolved in 17.3 µL of ammonium acetate buffer (250 mM, pH 5.5), and 9.6 MBq or 48.0 MBq of $^{111}InCl_3$ (370 MBq/mL, Mallinckrodt Medical, Petten, The Netherlands) was added for biodistribution or SPECT imaging, respectively. The mixture was shaken for 60 minutes at room temperature followed by addition of PBS (200 mM, pH 7.5). Of this mixture, 4.1 MBq or 20.7 MBq was added to 1.3 nmol or 0.7 nmol of N_3-Cy5-pLe^X-ω1 and stirred overnight at room temperature to form ^{111}In-DTPA -Cy5-pLe^X-ω1. The reaction mixture was directly used for injection.

SPECT imaging

10-week HFD-fed mice were injected intraperitoneally with 10 µg ^{111}In-DTPA-Cy5-pLe^X-ω1 (10 MBq/mouse). 24 hours post injection, *in vivo* biodistribution was assessed after the animals were placed and fixed on a dedicated positioned bed of a three-headed U-SPECT-2 (MILabs, Utrecht, The Netherlands) under continuous 1-2% isoflurane anesthesia. Radioactivity counts from total body scans and a second one of a head and neck area were acquired for 20 min and images were reconstructed as described before (58). After imaging, mice were euthanized by an intraperitoneal injection of 0.25 mL Euthasol (ASTfarma, Oudewater, The Netherlands).

Biodistribution

For biodistribution experiments, organs were harvested, weighed and radioactivity was counted (Wizard2 2470 automatic gamma scintillation counter, PerkinElmer, Groningen, the Netherlands). Total injected dose was determined by counting full and empty syringes in a gamma counter (2470 automatic gamma counter, Perkin-Elmer), and data are represented as % injected dose per gram tissue (%ID/g), which was calculated as follows: ((([MBq] tissue/[MBq]injected)*100)/g tissue).

Statistical analysis

All data are presented as mean ± standard error of the mean (SEM). Statistical analysis was performed using GraphPad Prism version 8 for Windows (GraphPad Software, La Jolla, CA, USA) with unpaired t-test, or either one-way or two-way analysis of variance (ANOVA) followed by Fisher's post-hoc test. Differences between groups were considered statistically significant at $P < 0.05$.

Acknowledgements

The authors thank Gerard van der Zon and Tessa Buckle (Leiden University Medical Center, Leiden, the Netherlands), and Uma Mahesh Gundra, Ada Weinstock, Jian-Da Lin and Mei San Tang (New York University School of Medicine, New York, USA) for their invaluable technical assistance. The authors also thank Ko Willems van Dijk and Patrick Rensen (Leiden University Medical Center) for allowing the use of the LUMC metabolic phenotyping platform (MRI and metabolic cages). This study was supported by Dutch Organization for Scientific Research (NWO; ZonMW TOP Grant 91214131 to CH, AS, MY and BG) and the NWO Graduate School Program (022.006.010 to HvdZ). This work was also supported in part by the Division of Intramural Research, National Institutes of Health (NIH)/National Institute of Allergy and Infectious Diseases (NIAID) and Awards AI130945 and AI133977, NIH/National Heart, Lung, and Blood Institute Award HL084312, and U.S. Department of Defense Award W81XWH-16-1-0256 (to PL). The funders had no role in study design, data collection and analysis, decision to publish, or preparation of the manuscript.

Conflict of interest

The authors have stated there are no conflicts of interest in connection with this article.

References

1. Donath MY, Shoelson SE. Type 2 diabetes as an inflammatory disease. Nat Rev Immunol. 2011;11(2):98-107.
2. Lackey DE, Olefsky JM. Regulation of metabolism by the innate immune system. Nat Rev Endocrinol. 2016;12(1):15-28.
3. Kolb H, Mandrup-Poulsen T. The global diabetes epidemic as a consequence of lifestyle-induced low-grade inflammation. Diabetologia. 2010;53(1):10-20.
4. Lumeng CN, DelProposto JB, Westcott DJ, Saltiel AR. Phenotypic switching of adipose tissue macrophages with obesity is generated by spatiotemporal differences in macrophage subtypes. Diabetes. 2008;57(12):3239-46.
5. Obstfeld AE, Sugaru E, Thearle M, Francisco AM, Gayet C, Ginsberg HN, et al. C-C chemokine receptor 2 (CCR2) regulates the hepatic recruitment of myeloid cells that promote obesity-induced hepatic steatosis. Diabetes. 2010;59(4):916-25.
6. Kratz M, Coats BR, Hisert KB, Hagman D, Mutskov V, Peris E, et al. Metabolic dysfunction drives a mechanistically distinct proinflammatory phenotype in adipose tissue macrophages. Cell Metab. 2014;20(4):614-25.
7. Lanthier N, Molendi-Coste O, Horsmans Y, van Rooijen N, Cani PD, Leclercq IA. Kupffer cell activation is a causal factor for hepatic insulin resistance. Am J Physiol Gastrointest Liver Physiol. 2010;298(1):G107-16.
8. Talukdar S, Oh DY, Bandyopadhyay G, Li D, Xu J, McNelis J, et al. Neutrophils mediate insulin resistance in mice fed a high-fat diet through secreted elastase. Nat Med. 2012;18(9):1407-12.
9. Molofsky AB, Nussbaum JC, Liang HE, Van Dyken SJ, Cheng LE, Mohapatra A, et al. Innate lymphoid type 2 cells sustain visceral adipose tissue eosinophils and alternatively activated macrophages. J Exp Med. 2013;210(3):535-49.
10. Wu D, Molofsky AB, Liang HE, Ricardo-Gonzalez RR, Jouihan HA, Bando JK, et al. Eosinophils sustain adipose alternatively activated macrophages associated with glucose homeostasis. Science. 2011;332(6026):243-7.
11. van der Zande HJP, Zawistowska-Deniziak A, Guigas B. Immune Regulation of Metabolic Homeostasis by Helminths and Their Molecules. Trends Parasitol. 2019;35(10):795-808.
12. Maizels RM, Yazdanbakhsh M. Immune regulation by helminth parasites: cellular and molecular mechanisms. Nat Rev Immunol. 2003;3(9):733-44.
13. Zinsou JF, Janse JJ, Honpkehedji YY, Dejon-Agobe JC, Garcia-Tardon N, Hoekstra PT, et al. Schistosoma haematobium infection is associated with lower serum cholesterol levels and improved lipid profile in overweight/obese individuals. PLoS Negl Trop Dis. 2020;14(7):e0008464.
14. Hussaarts L, Garcia-Tardon N, van Beek L, Heemskerk MM, Haeberlein S, van der Zon GC, et al. Chronic helminth infection and helminth-derived egg antigens promote adipose tissue M2 macrophages and improve insulin sensitivity in obese mice. FASEB J. 2015;29(7):3027-39.
15. Okano M, Satoskar AR, Nishizaki K, Abe M, Harn DA, Jr. Induction of Th2 responses and IgE is largely due to carbohydrates functioning as adjuvants on Schistosoma mansoni egg antigens. J Immunol. 1999;163(12):6712-7.

16. Hussaarts L, Yazdanbakhsh M, Guigas B. Priming dendritic cells for th2 polarization: lessons learned from helminths and implications for metabolic disorders. Front Immunol. 2014;5:499.

17. Everts B, Perona-Wright G, Smits HH, Hokke CH, van der Ham AJ, Fitzsimmons CM, et al. Omega-1, a glycoprotein secreted by Schistosoma mansoni eggs, drives Th2 responses. J Exp Med. 2009;206(8):1673-80.

18. Everts B, Hussaarts L, Driessen NN, Meevissen MH, Schramm G, van der Ham AJ, et al. Schistosome-derived omega-1 drives Th2 polarization by suppressing protein synthesis following internalization by the mannose receptor. J Exp Med. 2012;209(10):1753-67, S1.

19. Hams E, Bermingham R, Wurlod FA, Hogan AE, O'Shea D, Preston RJ, et al. The helminth T2 RNase omega1 promotes metabolic homeostasis in an IL-33- and group 2 innate lymphoid cell-dependent mechanism. FASEB J. 2016;30(2):824-35.

20. Meevissen MH, Wuhrer M, Doenhoff MJ, Schramm G, Haas H, Deelder AM, et al. Structural characterization of glycans on omega-1, a major Schistosoma mansoni egg glycoprotein that drives Th2 responses. J Proteome Res. 2010;9(5):2630-42.

21. Wilbers RH, Westerhof LB, van Noort K, Obieglo K, Driessen NN, Everts B, et al. Production and glyco-engineering of immunomodulatory helminth glycoproteins in plants. Sci Rep. 2017;7:45910.

22. Takeda K, Tanaka T, Shi W, Matsumoto M, Minami M, Kashiwamura S, et al. Essential role of Stat6 in IL-4 signalling. Nature. 1996;380(6575):627-30.

23. Takeda K, Kamanaka M, Tanaka T, Kishimoto T, Akira S. Impaired IL-13-mediated functions of macrophages in STAT6-deficient mice. J Immunol. 1996;157(8):3220-2.

24. Bhargava P, Li C, Stanya KJ, Jacobi D, Dai L, Liu S, et al. Immunomodulatory glycan LNFPIII alleviates hepatosteatosis and insulin resistance through direct and indirect control of metabolic pathways. Nat Med. 2012;18(11):1665-72.

25. Gundra UM, Girgis NM, Gonzalez MA, San Tang M, Van Der Zande HJP, Lin JD, et al. Vitamin A mediates conversion of monocyte-derived macrophages into tissue-resident macrophages during alternative activation. Nat Immunol. 2017;18(6):642-53.

26. Van den Bossche J, O'Neill LA, Menon D. Macrophage Immunometabolism: Where Are We (Going)? Trends Immunol. 2017;38(6):395-406.

27. Ricardo-Gonzalez RR, Red Eagle A, Odegaard JI, Jouihan H, Morel CR, Heredia JE, et al. IL-4/STAT6 immune axis regulates peripheral nutrient metabolism and insulin sensitivity. Proc Natl Acad Sci U S A. 2010;107(52):22617-22.

28. Dunne DW, Lucas S, Bickle Q, Pearson S, Madgwick L, Bain J, et al. Identification and partial purification of an antigen (omega 1) from Schistosoma mansoni eggs which is putatively hepatotoxic in T-cell deprived mice. Trans R Soc Trop Med Hyg. 1981;75(1):54-71.

29. Abdulla MH, Lim KC, McKerrow JH, Caffrey CR. Proteomic identification of IPSE/alpha-1 as a major hepatotoxin secreted by Schistosoma mansoni eggs. PLoS Negl Trop Dis. 2011;5(10):e1368.

30. Gieseck RL, 3rd, Ramalingam TR, Hart KM, Vannella KM, Cantu DA, Lu WY, et al. Interleukin-13 Activates Distinct Cellular Pathways Leading to Ductular Reaction, Steatosis, and Fibrosis. Immunity. 2016;45(1):145-58.

31. Hart KM, Fabre T, Sciurba JC, Gieseck RL, 3rd, Borthwick LA, Vannella KM, et al. Type 2 immunity is protective in metabolic disease but exacerbates NAFLD collaboratively with TGF-beta. Sci Transl Med. 2017;9(396).

32. Schwartz MW, Woods SC, Porte D, Jr., Seeley RJ, Baskin DG. Central nervous system control of food intake. Nature. 2000;404(6778):661-71.

33. Schneeberger M, Gomis R, Claret M. Hypothalamic and brainstem neuronal circuits controlling homeostatic energy balance. J Endocrinol. 2014;220(2):T25-46.

34. Hummel KP, Dickie MM, Coleman DL. Diabetes, a new mutation in the mouse. Science. 1966;153(3740):1127-8.

35. de Ruiter K, Tahapary DL, Sartono E, Soewondo P, Supali T, Smit JWA, et al. Helminths, hygiene hypothesis and type 2 diabetes. Parasite Immunol. 2017;39(5).

36. Hadju V, Stephenson LS, Abadi K, Mohammed HO, Bowman DD, Parker RS. Improvements in appetite and growth in helminth-infected schoolboys three and seven weeks after a single dose of pyrantel pamoate. Parasitology. 1996;113 (Pt 5):497-504.

37. Lohmus M, Moalem S, Bjorklund M. Leptin, a tool of parasites? Biol Lett. 2012;8(5):849-52.

38. Horbury SR, Mercer JG, Chappell LH. Anorexia induced by the parasitic nematode, Nippostrongylus brasiliensis: effects on NPY and CRF gene expression in the rat hypothalamus. J Neuroendocrinol. 1995;7(11):867-73.

39. Murphy KG, Bloom SR. Gut hormones and the regulation of energy homeostasis. Nature. 2006;444(7121):854-9.

40. Li Z, Yi CX, Katiraei S, Kooijman S, Zhou E, Chung CK, et al. Butyrate reduces appetite and activates brown adipose tissue via the gut-brain neural circuit. Gut. 2018;67(7):1269-79.

41. Cai D, Liu T. Hypothalamic inflammation: a double-edged sword to nutritional diseases. Ann N Y Acad Sci. 2011;1243:E1-39.

42. Valdearcos M, Douglass JD, Robblee MM, Dorfman MD, Stifler DR, Bennett ML, et al. Microglial Inflammatory Signaling Orchestrates the Hypothalamic Immune Response to Dietary Excess and Mediates Obesity Susceptibility. Cell Metab. 2017;26(1):185-97 e3.

43. Lee CH, Kim HJ, Lee YS, Kang GM, Lim HS, Lee SH, et al. Hypothalamic Macrophage Inducible Nitric Oxide Synthase Mediates Obesity-Associated Hypothalamic Inflammation. Cell Rep. 2018;25(4):934-46 e5.

44. Cardoso V, Chesne J, Ribeiro H, Garcia-Cassani B, Carvalho T, Bouchery T, et al. Neuronal regulation of type 2 innate lymphoid cells via neuromedin U. Nature. 2017;549(7671):277-81.

45. Klose CSN, Mahlakoiv T, Moeller JB, Rankin LC, Flamar AL, Kabata H, et al. The neuropeptide neuromedin U stimulates innate lymphoid cells and type 2 inflammation. Nature. 2017;549(7671):282-6.

46. Wallrapp A, Riesenfeld SJ, Burkett PR, Abdulnour RE, Nyman J, Dionne D, et al. The neuropeptide NMU amplifies ILC2-driven allergic lung inflammation. Nature. 2017;549(7672):351-6.

47. Hanada R, Teranishi H, Pearson JT, Kurokawa M, Hosoda H, Fukushima N, et al. Neuromedin U has a novel anorexigenic effect independent of the leptin signaling pathway. Nat Med. 2004;10(10):1067-73.

48. Kaisar MMM, Ritter M, Del Fresno C, Jonasdottir HS, van der Ham AJ, Pelgrom LR, et al. Dectin-1/2-induced autocrine PGE2 signaling licenses dendritic cells to prime Th2 responses. PLoS Biol. 2018;16(4):e2005504.

49. Grogan JL, Kremsner PG, Deelder AM, Yazdanbakhsh M. Elevated proliferation and interleukin-4 release from CD4+ cells after chemotherapy in human Schistosoma haematobium infection. Eur J Immunol. 1996;26(6):1365-70.

50. Lee S, Muniyappa R, Yan X, Chen H, Yue LQ, Hong EG, et al. Comparison between surrogate indexes of insulin sensitivity and resistance and hyperinsulinemic euglycemic clamp estimates in mice. Am J Physiol Endocrinol Metab. 2008;294(2):E261-70.

51. Stephenne X, Foretz M, Taleux N, van der Zon GC, Sokal E, Hue L, et al. Metformin activates AMP-activated protein kinase in primary human hepatocytes by decreasing cellular energy status. Diabetologia. 2011;54(12):3101-10.

52. Hashimshony T, Senderovich N, Avital G, Klochendler A, de Leeuw Y, Anavy L, et al. CEL-Seq2: sensitive highly-multiplexed single-cell RNA-Seq. Genome Biol. 2016;17:77.

53. Langmead B, Salzberg SL. Fast gapped-read alignment with Bowtie 2. Nat Methods. 2012;9(4):357-9.

54. Anders S, Pyl PT, Huber W. HTSeq--a Python framework to work with high-throughput sequencing data. Bioinformatics. 2015;31(2):166-9.

55. Thomas A, Belaidi E, Aron-Wisnewsky J, van der Zon GC, Levy P, Clement K, et al. Hypoxia-inducible factor prolyl hydroxylase 1 (PHD1) deficiency promotes hepatic steatosis and liver-specific insulin resistance in mice. Sci Rep. 2016;6:24618.

56. Kleiner DE, Brunt EM, Van Natta M, Behling C, Contos MJ, Cummings OW, et al. Design and validation of a histological scoring system for nonalcoholic fatty liver disease. Hepatology. 2005;41(6):1313-21.

57. Hensbergen AW, van Willigen DM, Welling MM, van der Wijk FA, de Korne CM, van Oosterom MN, et al. Click Chemistry in the Design and Production of Hybrid Tracers. ACS Omega. 2019;4(7):12438-48.

58. Spa SJ, Welling MM, van Oosterom MN, Rietbergen DDD, Burgmans MC, Verboom W, et al. A Supramolecular Approach for Liver Radioembolization. Theranostics. 2018;8(9):2377-86.

Supplementary information

Supplementary Table 1. Antibodies and reagents for flow cytometry.

Target	Clone	Conjugate	Source	Identifier
B220	RA3-6B2	FITC	eBioscience	11-0452
CD3	17A2	Alexa Fluor 700	Biolegend	100216
CD3	17A2	APC-eF780	eBioscience	47-0032
CD3	17A2	eF450	eBioscience	48-0032
CD3	17A2	FITC	eBioscience	11-0032
CD4	GK1.5	PE-Cy7	eBioscience	25-0041
CD4	GK1.5	PerCP-eF710	eBioscience	46-0041
CD11b	M1/70	APC-Cy7	Biolegend	101226
CD11b	M1/70	FITC	eBioscience	11-0112
CD11b	M1/70	PE-Cy7	eBioscience	25-0112
CD11c	N418	BV421	Biolegend	117330
CD11c	HL3	HV450	BD Biosciences	560521
CD19	6D5	Alexa Fluor 700	Biolegend	115528
CD45	30-F11	BV785	Biolegend	103149
CD45.2	104	FITC	Biolegend	109806
CD45.2	104	eF450	eBioscience	48-0454
CD45.2	104	PerCP-Cy5.5	Tonbo Biosciences	65-0454
F4/80	BM8	APC	eBioscience	17-4801
F4/80	BM8	PE-Cy7	Biolegend	123114
F4/80	BM8	BV711	Biolegend	123147
Foxp3	FJK-16s	PE	eBioscience	12-5773
GR-1	RB6-8C5	FITC	BD Biosciences	553126
IFN-γ	XMG1.2	APC	eBioscience	17-7311
IL-4	11B11	APC	eBioscience	17-7041
IL-5	TRFK5	PE	Biolegend	504303
IL-13	eBio13A	eF450	eBioscience	48-7133
Ly6C	HK1.4	Alexa Fluor 700	Biolegend	128024
Ly6C	HK1.4	APC-Cy7	Biolegend	128026
NK1.1	PK136	Alexa Fluor 700	Biolegend	108730
NK1.1	PK136	FITC	eBioscience	11-5941
Siglec-F	E50-2440	BV421	BD Biosciences	562681
Siglec-F	E50-2440	BV605	BD Biosciences	740388
Siglec-F	E50-2440	PE	BD Biosciences	552126
Thy1.2	53-2.1	APC-eF780	eBioscience	47-0902
YM1	Polyclonal	Biotin	R&D Systems	BAF2446
Other reagents			**Source**	**Identifier**
CM-H2DCFDA			Invitrogen	C6827
LIVE/DEAD™ Fixable Aqua Dead Cell Stain Kit			Invitrogen	L34957
LIVE/DEAD™ Fixable Blue Dead Cell Stain Kit			Invitrogen	L23105
MitoTracker™ Green FM			Invitrogen	M7514
Streptavidin-PerCP			BD Biosciences	554064
Streptavidin-PerCP-Cy5.5			Biolegend	405214
TMRM			Invitrogen	T668
Zombie UV™ Fixable Viability Kit			Biolegend	423107

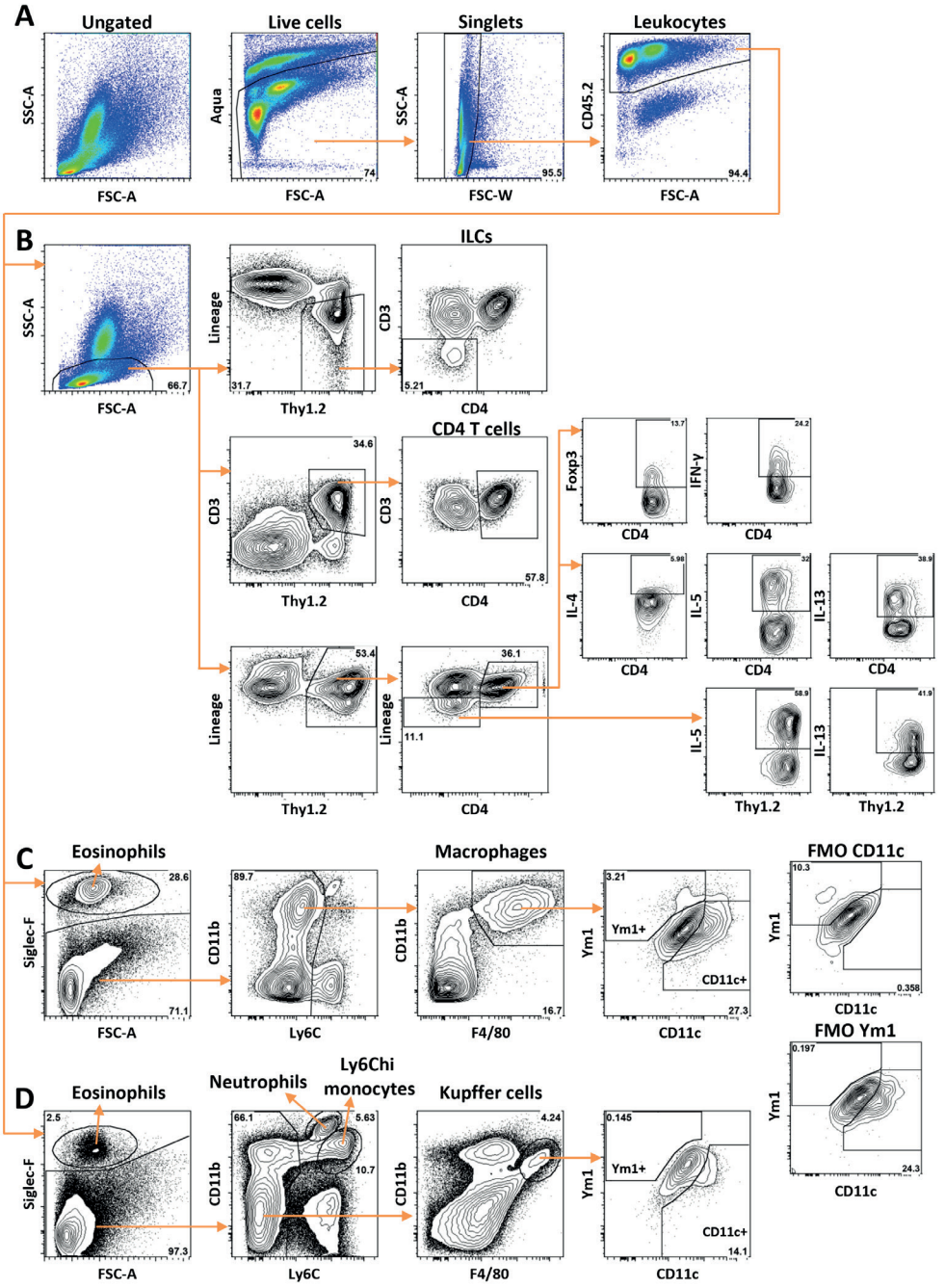

Supplementary Figure 1. Gating strategies. (**A**) Isolated cells were pre-gated on Aqua^{-}CD45^{+} single cells. (**B**) The gating strategy for eWAT and liver analyses of ILCs, CD4 T cells and intracellular cytokine production is shown. The lineage channel includes antibodies against CD11b, CD11c, B220,

◀Supplementary Figure 1. Legend (Continued)

GR-1, NK1.1 and CD3. (**C**) The gating strategies for eWAT eosinophils, $CD11c^{+}YM1^{-}$ macrophages and $CD11c^{-}YM1^{+}$ macrophages are shown, including Fluorescence Minus One (FMO) controls for CD11c and Ym1. (**D**) The gating strategy for liver eosinophils, monocytes, $CD11c^{+}YM1^{-}$ Kupffer cells and $CD11c^{-}YM1^{+}$ Kupffer cells is shown.

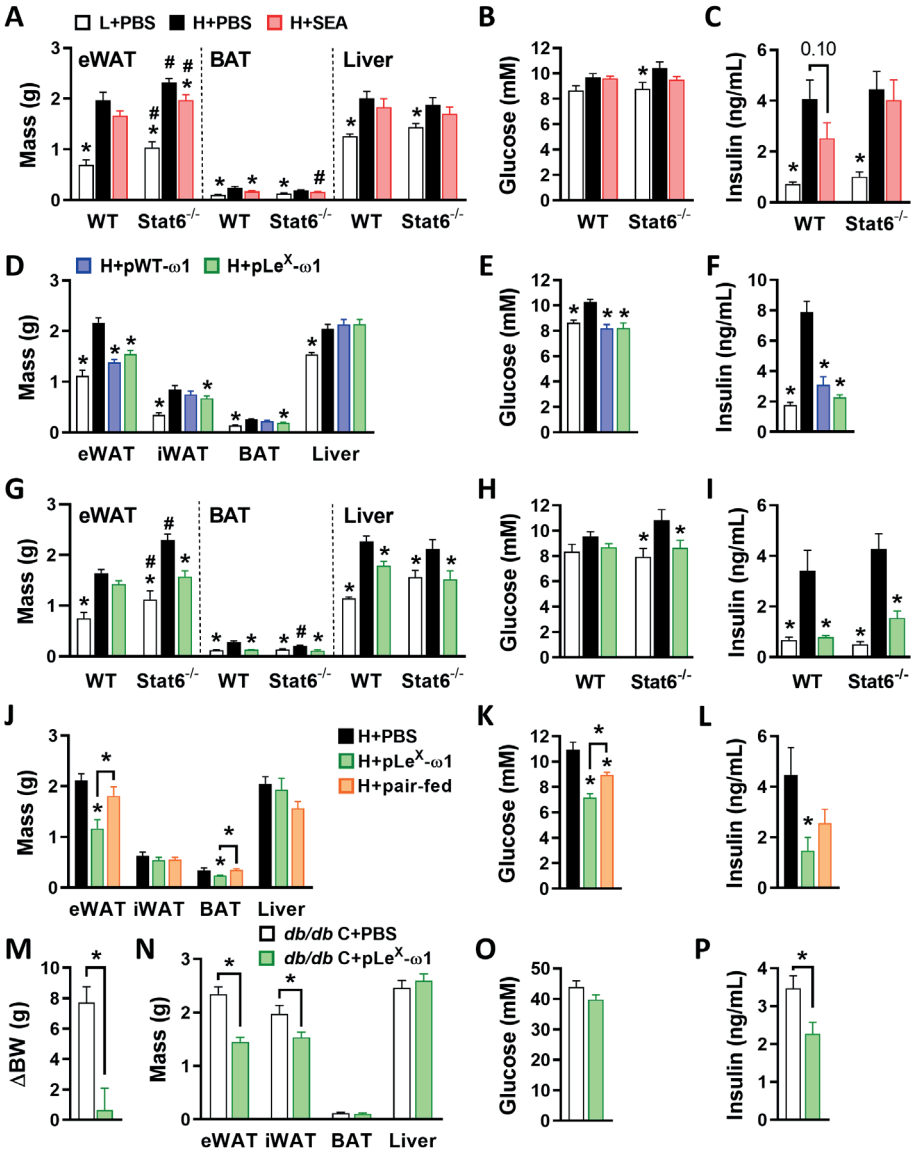

Supplementary Figure 2. Body composition and fasting blood glucose and plasma insulin levels after SEA and pLeX-ω1 treatment in obese mice. (**A-P**) Supplementary data for Figure 1 (*A-C*), 3 (*D-F*), 4 (*G-I*), 5 (*J-L*) and 6 (*M-P*). Mice were fed a LFD or a HFD and treated as described in the corresponding figure legends. The weights of epididymal WAT (eWAT), inguinal WAT (iWAT), intrascapular brown adipose tissue (BAT) and the liver were measured after 4 weeks (*A, D, G, J* and *N*). Blood glucose (*B, E, H, K* and *O*) and plasma insulin (*C, F, I, L* and *P*) were measured at week 4 in 4h-fasted mice. Body weight change after 4 weeks was determined in *db/db* mice treated with PBS or 50 µg pLe^{X}-ω1 (*M*). Results are expressed as means ± SEM. **P*<0.05 *vs* HFD or as indicated, #*P*<0.05 *vs* WT (n = 3-6 mice per group in A-C, G-P and 11-18 mice per group in D-F).

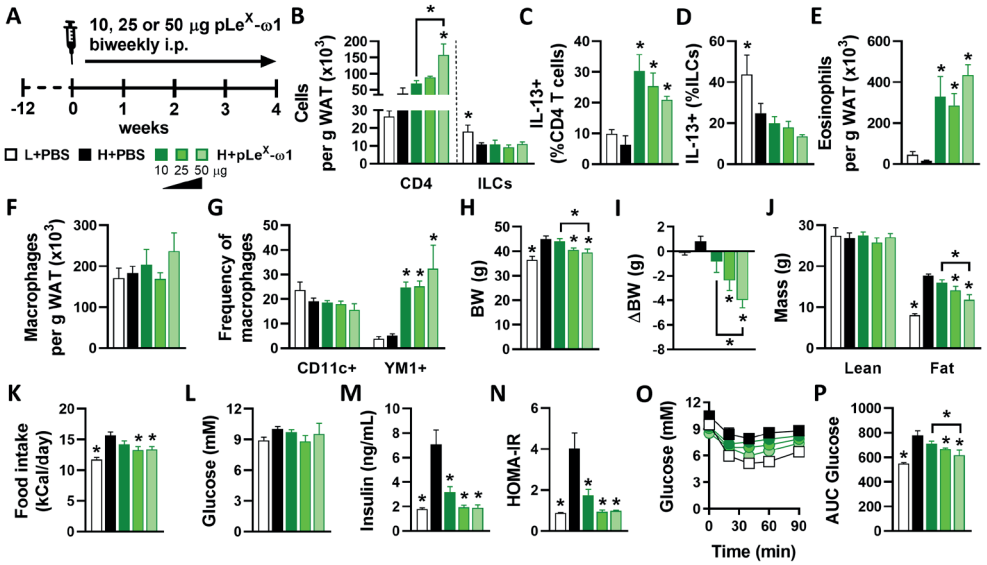

Supplementary Figure 3. pLeX-ω1 increases adipose tissue type 2 immune cells and improves whole-body insulin sensitivity in a dose-dependent manner. (**A**) Mice were fed a LFD (white bars) or a HFD for 12 weeks, and next received biweekly intraperitoneal injections of PBS (black bars) or 10 µg, 25 µg or 50 µg pLe^{X}-ω1 (green bars) for 4 weeks. At the end of the experiment, eWAT was collected, processed and analyzed as described in the legend of Figure 1. (**B-G**) The numbers of CD4 T cells and ILCs per gram tissue (*B*), and the frequencies of IL-13^{+} CD4 T cells (*C*) and ILCs (*D*) were determined. Numbers of eosinophils (*E*) and macrophages (*F*) per gram tissue, and percentages of CD11c^{+}YM1^{-} and CD11c^{-}YM1^{+} macrophages (*G*) were determined. (**H-J**) Body weight (*H-I*) and body composition (*J*) were determined after 4 weeks. (**K**) Food intake was monitored throughout the treatment period. (**L-N**) Fasting blood glucose (*L*) and plasma insulin levels (*M*) were determined at week 4, and HOMA-IR (*N*) was calculated. (**O-P**) An i.p. insulin tolerance test (*O-P*) was performed at week 3. Results are expressed as means ± SEM. * *P*<0.05 *vs* HFD or as indicated (n = 3-4 mice per group).

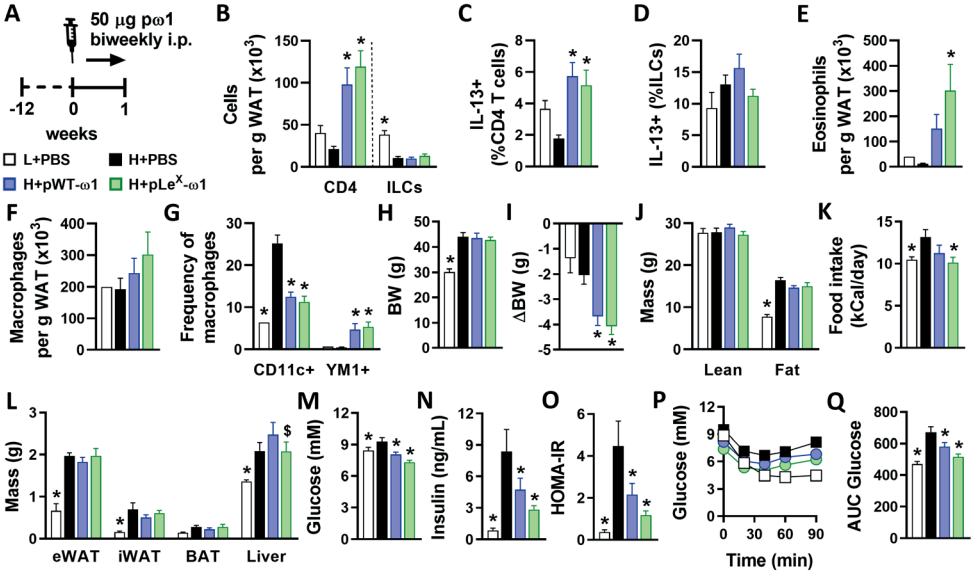

Supplementary Figure 4. ω1 glycovariants increase adipose tissue type 2 immune cells and improve whole-body insulin sensitivity after 1 week of treatment. (**A**) Mice were fed a LFD (white bars) or a HFD for 12 weeks, and next received biweekly intraperitoneal injections of PBS (black bars) or 50 µg pWT-ω1 (blue bars) or pLe^{X}-ω1 (green bars) for 1 week. At the end of the experiment, eWAT was collected, processed and analyzed as described in the legend of Figure 1. (**B-G**) The numbers of CD4 T cells and ILCs per gram tissue (*B*), and the frequencies of IL-13^{+} CD4 T cells (*C*) and ILCs (*D*) were determined. Numbers of eosinophils (*E*) and macrophages (*F*) per gram tissue, and frequencies of CD11c^{+}YM1^{-} and CD11c^{-}YM1^{+} macrophages (*G*) were determined. (**H-L**) Body weight (*H*), body weight change (*I*), body composition (*J, L*) and food intake (*K*) were measured after 1 week of treatment. (**M-O**) Fasting blood glucose (*M*) and plasma insulin levels (*N*) were determined in 4h-fasted mice at the end of week 1, and HOMA-IR (*O*) was calculated. (**P-Q**) An i.p. insulin tolerance test was performed. Results are expressed as means ± SEM. **P*<0.05 *vs* HFD, $*P*<0.05 *vs* pWT-ω1 (n = 1-9 mice per group).

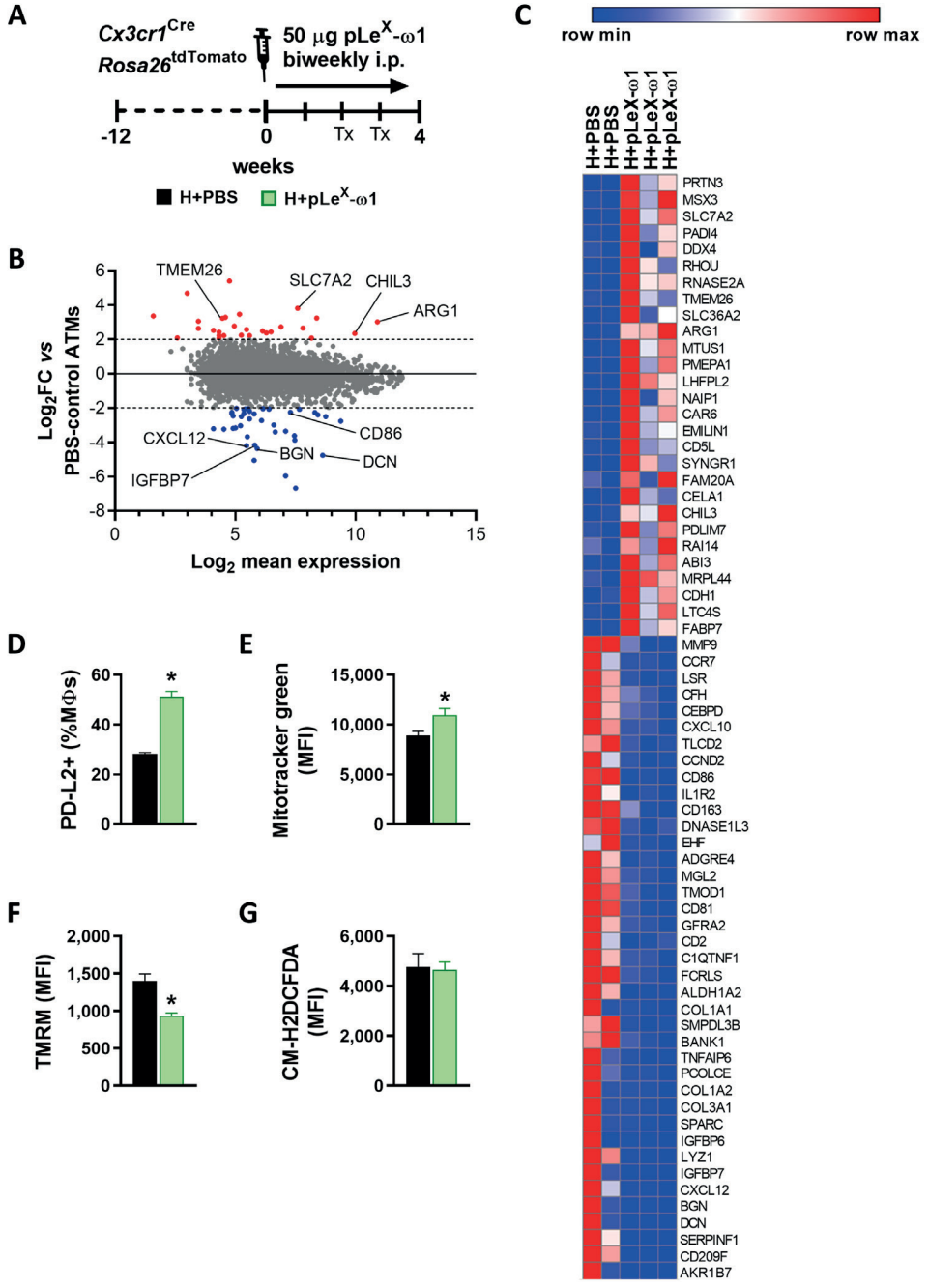

Supplementary Figure 5. Adipose tissue macrophages from mice treated with pLeX-ω1 display some alternatively-activated phenotypic features. (**A**) *Cx3cr1*^{CreER} *R26*^{tdTomato} mice were fed a HFD

▲Supplementary Figure 5. Legend (Continued)

for 12 weeks, and next received biweekly intraperitoneal injections of PBS or 50 μg pLe^{X}-ω1 for 4 weeks. At week 2 and 3, mice received an oral gavage with tamoxifen (Tx) to label CX3CR1^{+} cells. At the end of the experiment, adipose tissue macrophages (ATMs) from eWAT SVF were FACS-sorted and RNA was isolated and sequenced. (**B**) MA plot shows the mean gene expression in pLe^{X}-ω1 ATMs, as expressed in $\log_2$ fold change *versus* PBS-control ATMs. Upregulated genes ($\log_2$ fold change > 2) are indicated in red and downregulated genes ($\log_2$ fold change < -2) are indicated in blue. (**C**) Normalized read counts of upregulated and downregulated genes are visualized in a heatmap. (**D-G**) WT mice were fed a HFD for 12 weeks, and next received biweekly intraperitoneal injections of PBS (black bars) or 50 μg pLe^{X}-ω1 (green bars) for 4 weeks. Percentage of PD-L2^{+} macrophages (*D*) was determined. MitoTracker Green (mitochondrial mass; *E*), TMRM (mitochondrial membrane potential; *F*) and CM-H2CFDA (total ROS; *G*) fluorescence intensities were determined in PD-L2^{+} macrophages. Results are expressed as means ± SEM. *P<0.05 *vs* HFD (n = 2-3 mice per group in B-C, and 3-4 mice per group in D-G).

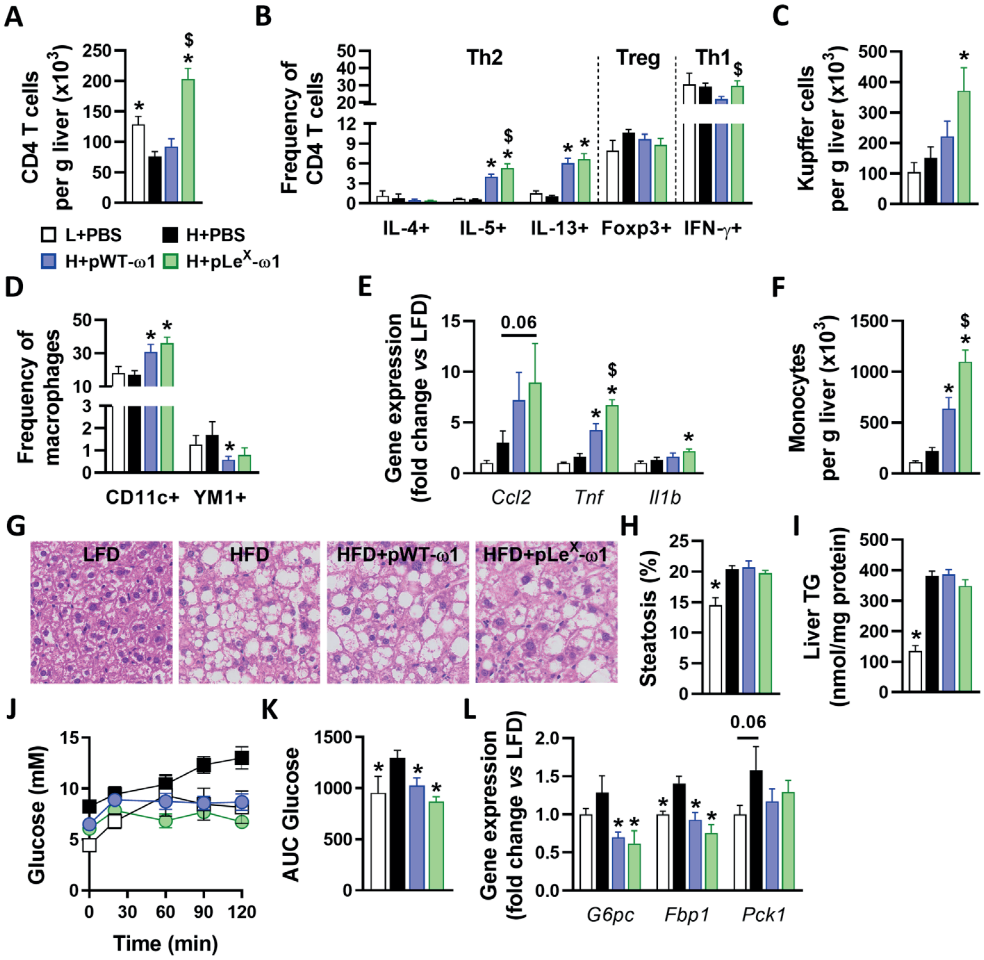

Supplementary Figure 6. ω1 glycovariants do not affect hepatic steatosis, but reduce gluconeogenesis in obese mice. Mice were fed a LFD (white bars) or a HFD for 12 weeks, and next received biweekly intraperitoneal injections of PBS (black bars) or 50 µg pWT-ω1 (blue bars) or pLe^{X}-ω1 (green bars) for 4 weeks, as described in the legend of Figure 2. At sacrifice, CD45^{+} liver cells were isolated and analyzed by flow cytometry. (**A-F**) The numbers of CD4 T cells (*A*), Kupffer cells (KC, *C*) and Ly6C^{hi} monocytes (*F*) per gram tissue, and the frequencies of T helper (*B*) and KC subsets (*D*) were determined. The mRNA expression of proinflammatory genes (*E*) was determined. (**G-I**) Hepatic steatosis was assessed using hematoxylin/eosin staining in fixed tissues (*G-H*) and hepatic triglycerides content was determined (*I*). (**J-K**) An intraperitoneal pyruvate tolerance test was performed during week 4. Blood glucose levels were measured at the indicated time points (*J*) and the AUC of the glucose excursion curve was calculated (*K*). (**L**) The mRNA expression of the main gluconeogenic genes was determined. Data shown are a pool of at least two independent experiments, except for J-K. Results are expressed as means ± SEM. *P<0.05 *vs* HFD, \$$P$<0.05 *vs* pWT-ω1 (n = 5-18 mice per group in A-I, L, and 3-6 mice per group in J-K).

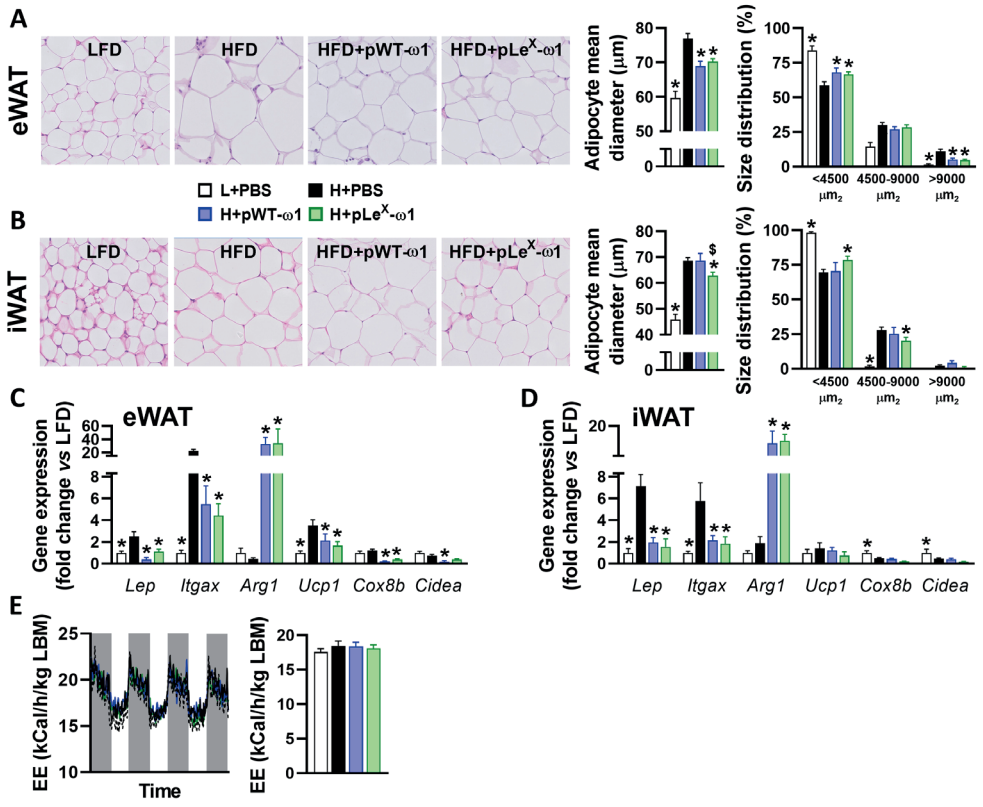

Supplementary Figure 7. ω1 glycovariants reduce adipocyte size, but neither increase adipose tissue beiging nor whole-body energy expenditure in obese mice. (**A-D**) Mice were fed a LFD (white bars) or a HFD for 12 weeks, and next received biweekly intraperitoneal injections of PBS (black bars) or 50 µg pWT-ω1 (blue bars) or pLe^X-ω1 (green bars) as described in the legend of Figure 2. At sacrifice, the eWAT (*A,C*) or iWAT (*B,D*) were collected. Adipocyte diameter and size distribution were determined after H&E staining (*A,B*). mRNA expressions of the indicated genes were determined by RT-PCR and expressed relative to the *RplP0* gene as fold change versus LFD-fed mice (*C,D*). (**E**) Energy expenditure, corrected for lean body mass, was measured for three consecutive days using fully automated single-housed metabolic cages during the first week of treatment. Data shown are a pool of two independent experiments. Results are expressed as means ± SEM. *P<0.05 *vs* HFD (n = 4-10 mice per group).

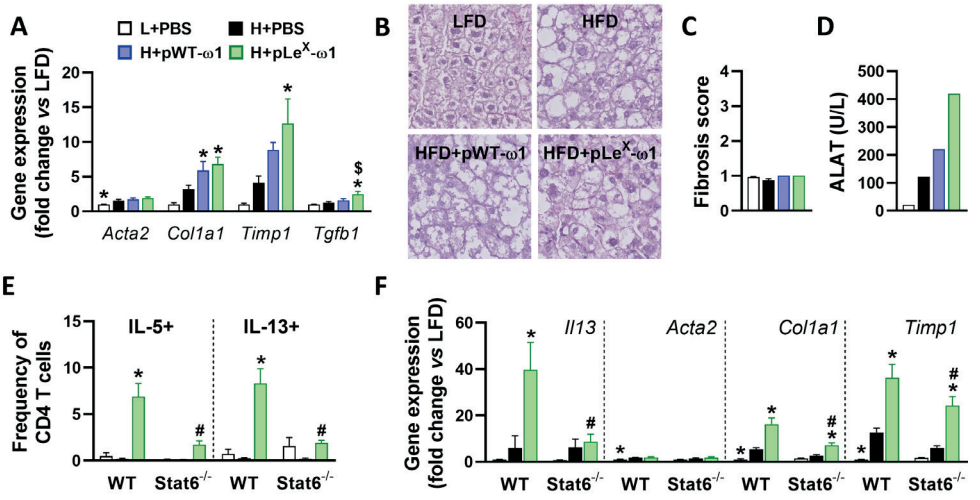

Supplementary Figure 8. ω1 glycovariants increase fibrosis gene markers and liver damage in obese mice. Mice were fed a LFD (white bars) or a HFD for 12 weeks, and next received biweekly intraperitoneal injections of PBS (black bars) or 50 µg pWT-ω1 (blue bars) or pLe^{X}-ω1 (green bars) for 4 weeks, as described in the legend of Figure 2. (**A**) The mRNA expression of fibrosis gene markers was determined. (**B-C**) Sirius Red-stained sections of fixed tissues (*B*) were scored for fibrosis (*C*). (**D**) Plasma alanine aminotransferase levels were determined at week 4. (**E-F**) WT and *Stat6*$^{-/-}$ mice were fed a LFD or a HFD and next received biweekly intraperitoneal injections of PBS or 50 µg pWT/pLeX-ω1 for 4 weeks, as described in the legend of Figure 4. Hepatic frequencies of IL-5 and IL-13-expressing CD4 T cells (*E*), and mRNA expression of *Il13* and fibrosis gene markers (*F*) were determined. Data shown are a pool of at least two independent experiments, except for E-F. Results are expressed as means ± SEM. **P*<0.05 *vs* HFD, $*P*<0.05 *vs* pWT-ω1, #*P*<0.05 *vs* WT (n = 5-18 mice per group in A-D, and 3-5 mice per group in E-F).

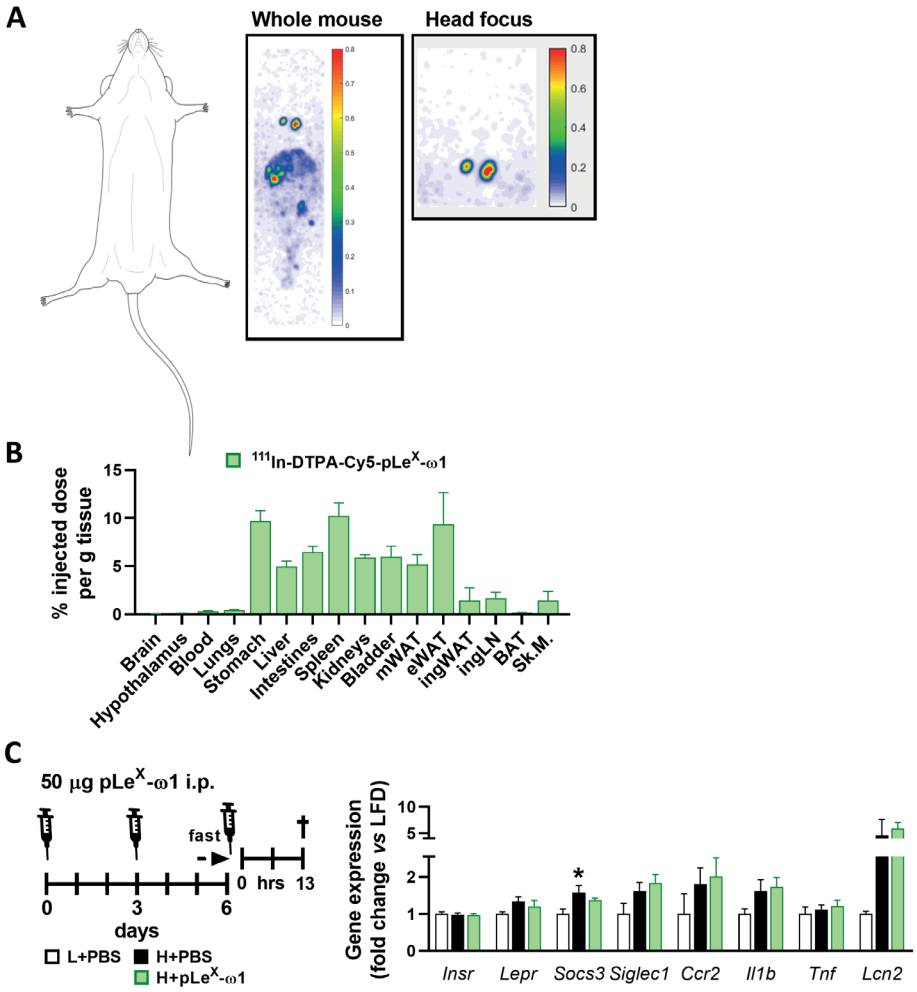

Supplementary Figure 9. Fluorescent and radioactive hybrid-labelled pLeX-ω1 distributes to abdominal organs, but not to the brain; pLeX-ω1 does not affect HFD-induced hypothalamic inflammation. (**A-B**) Mice were fed a HFD for 12 weeks, and next received a single intraperitoneal injection of 10 µg of either 1 (*A*) or 10 (*B*) MBq ^{111}In-DTPA-Cy5-pLe^{X}-ω1. After 24h, the biodistribution was visualized by SPECT scan of the whole mouse (*A*), with a head focus (*insert*), and organs were collected and weighed after sacrifice. The organ-specific ^{111}In radioactivity was counted and data expressed as mean % injected dose per g tissue ± SEM (*B*; n = 6 mice per group). (**C**) Mice were fed a LFD (white bars) or HFD (black/green bars) for 12 weeks and fasted prior to intraperitoneal injections of either PBS (white/black bars) or 50 µg pLeX-ω1 (green bars; *C*). The hypothalami were collected and freeze-clamped 13h post-injection, at the peak of the inhibitory effect observed on food intake during the dark phase (see Figure 5). mRNA expression of the indicated genes (*C*) was determined by RT-PCR and expressed relative to the *RplP0* gene as fold change versus LFD-fed mice. Results are expressed as means ± SEM. *P<0.05 vs HFD (n = 4-6 mice per group).